PROJECT THOR ABLE-4
FINAL MISSION REPORT

25 May 1960

Prepared by
Flight Test Planning and Evaluation Section
Experimental Space Projects Office

Approved: P. F. Thiel
for A. K. Thiel
Program Director
Experimental Space Projects

SPACE TECHNOLOGY LABORATORIES, INC.
P. O. Box 95001
Los Angeles 45, California

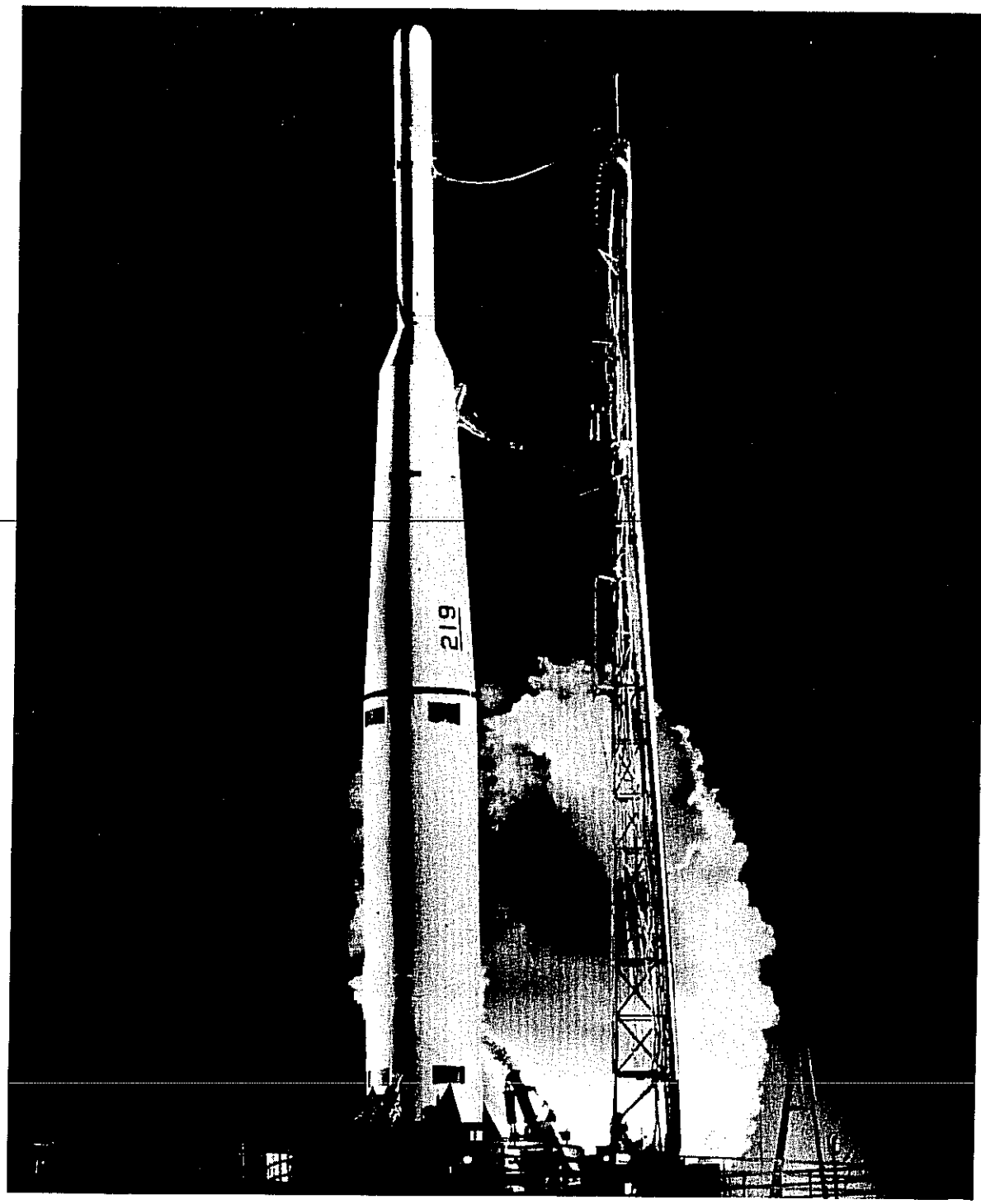
219

PREFACE

This is the first volume of a two-volume final report by Space Technology Laboratories, Inc., in the launch and operation of the Able-4 satellite (1960α or Pioneer V). Final information on the Able-4 four-stage test vehicle is given in this volume. The second volume, which will be concerned exclusively with the scientific results of the program, will be issued when these results are known in sufficient detail; however, a preliminary review is given in Section 6 of this volume.

CONTENTS

CONTENTS (Continued)

ILLUSTRATIONS

ILLUSTRATIONS (Cont.)

TABLES

1. SUMMARY

The THOR ABLE-4 test vehicle was launched from Stand 17A at Cape Canaveral Missile Test Annex on 11 March 1960 at 0800:06.99 EST. Shortly after lift-off, it was roll programmed to a flight heading of 88 degrees True. All stages of the vehicle operated satisfactorily and the payload was injected into an elliptical orbit about the sun as planned. The trajectory was designed to enable the payload to pass as close to the sun as vehicle performance permitted. Ecliptic elements of the heliocentric orbit (see Section 5, Figure 5-4) are as follows:

a = 0.89958 A.U. (semimajor axis)
e = 0.10396 (eccentricity)
i = 3.351 degrees (inclination of orbit plane to ecliptic)
Ω = -10.288 degrees (longitude of ascending node from vernal equinox)
ω = -2.585 degrees (angle in orbit plane from ascending node to perigee)
t = 151.96 days (time from T_o to perihelion)
311.64 days (period)
0.8061 A.U. (perihelion)
0.9931 A.U. (aphelion)

Essentially all major test objectives of the flight were achieved, and invaluable scientific data is being obtained daily from the payload experiments. Significant data was obtained from the ion chamber and Geiger counter during solar flare activity beginning 31 March. The magnetometer experiment has enabled discovery of a third major dynamic element of charged particles surrounding the earth, in addition to providing more data on the inner and outer Van Allen radiation belts. It also has enabled measurement of the interplanetary magnetic field and disclosed that the intense zone of disturbed magnetic fields, postulated to be the boundary between the earth's magnetic field and magnetic fields which accompany plasma emitted from the sun, is apparently twice as far from the earth

as previously supposed. The cosmic ray experiment has obtained invaluable data relative to solar flare activity during flight of the payload Tracking schedules have been changed at times to exploit gathering of such data during periods of solar flare activity. The aspect indicator has not provided usable information. Usefulness of data from the micrometeorite experience is questionable. Calculation of the Astronomical Unit is expected to be made at a later date.

Several discrepancies in vehicle performance during powered flight, which were not significant to this mission, were extensively studied because of their possible effect on future missions with similar hardware. Noise in the guidance system tracking data resulted in an undesirable pitch-up command and overcorrection in yaw. An angular turning rate beginning at SECO resulted in a discontinuity in attitude between second- and third-stage velocity vectors.

The payload transmitter and command system has operated perfectly since launch. All transmissions from launch until 8 May were made using five watts power from the payload. On 8 May, the payload power amplifier was turned on for the first time to provide 150 watts power output. The payload temperature control is working very satisfactorily. A continuing degradation of the duty cycle of the batteries used in the solar power supply system has been experienced sinch launch, such that power presently available is approximately 15 percent of that available at lift-off.

The worldwide network of STL tracking stations has participated very successfully on this project. Two-way communication with a space vehicle has been accomplished over far greater ranges than ever achieved previously. The stations at South Point, Hawaii, and Manchester, England, are maintaining daily contact with the payload. Provided continued operation is available from the batteries, it is expected that communication with the payload will be maintained until the probe reaches a distance of 20 million miles from the earth (see Figure 1-1) with the 5-watt transmitter. Battery degradation has eliminated the possibility of further 150-watt operations.

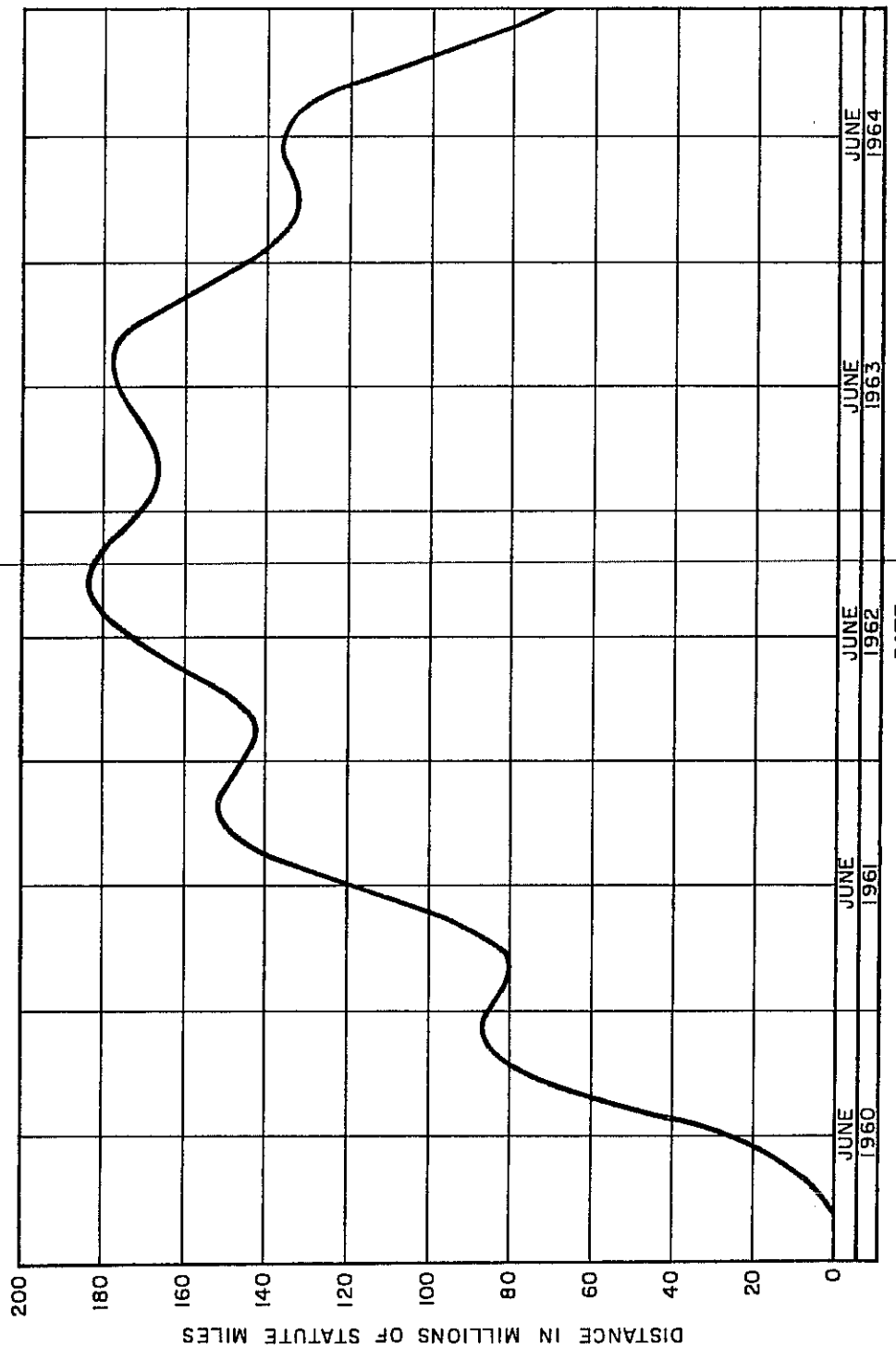

Figure 1-1. Thor Able-4 Distance from Earth Versus Date.

2. ACHIEVEMENT OF OBJECTIVES

Test objectives for the THOR ABLE-4 launch and the extent to which these objectives have been achieved are as follows:

2.1 Primary Test Objectives

2.1.1 Objective

Launch of an instrument probe beyond the immediate gravitational field of the earth and into deep space in order to obtain scientific data for extension of our knowledge of the solar system.

Objective Achieved

Payload telemetry data is providing valuable information on micrometeorite flux, magnetic field, radiation density, and temperatures. The tracking data may permit a more precise measurement of the astronomical unit.

2.1.2 Objective

Guide an instrumented probe along a trajectory enabling it to approach the orbital path of the planet Venus and become an artificial planet in elliptical orbit about the sun.

Objective Achieved

Payload has been delivered in operating condition along a trajectory which will permit it to approach the orbit of the planet Venus and become an instrumented planet in an elliptical orbit about the sun.

2.1.3 Objective

Demonstrate the capability of ground tracking stations to track and to receive telemetered information from a deep space probe vehicle.

Objective Achieved

Payload telemetry has been received and tracked by stations in a worldwide network, with two-way communications accomplished over distances far exceeding any previous tests.

2.1.4 Objective

Demonstrate the capability of the Stage II guidance system to steer a test vehicle and terminate Stage II propulsion with sufficient accuracy for intercontinental and interplanetary flights.

Objective Essentially Achieved

Performance of the Stage II guidance system was satisfactory for this flight; however, certain discrepancies were noted which require correction on future flights. (See Section 4.3.3).

2.1.5 Objective

Evaluate the suitability of the planned trajectory for flying to the orbit of the planet Venus.

Objective Achieved

It has been demonstrated that the planned trajectory is suitable for flying to the orbit of the planet Venus.

2.2 Secondary Test Objectives

2.2.1 Objective

Determine operation of the Stage I/II, II/III, and III/Payload separation mechanisms.

Objective Achieved

All separation mechanisms performed satisfactorily.

2.2.2 Objective

Evaluate the ability of the Stage II flight control system to maintain proper attitude control.

Objective Achieved

The flight control system maintained attitude control within the design limits throughout second-stage burning.

2.2.3 Objective

Evaluate performance of the Stage II Aerojet-General Corporation AJ10-101A propulsion system.

Objective Achieved

The second-stage propulsion system performed satisfactorily and propulsion was terminated by the guidance system at the required velocity.

2.2.4 Objective

Demonstrate satisfactory performance of Stage II spin rockets in providing spin stabilization for Stage III and the payload.

Objective Achieved

Second-stage spin rockets provided adequate spinrate, and spin stabilization of the third stage and payload is considered satisfactory.

2.2.5 Objective

Determine performance of the Stage III Allegany Ballistics Laboratory (ABL)X248-A4 solid-propellant rocket.

Objective Achieved

Performance of the third-stage solid-propellant rocket was very close to nominal.

2.2.6 Objective

Determine the performance and operation of the payload solar cell and battery system.

Objective Achieved

The payload solar cell and battery system initially provided satisfactory power to the experiments and telemetry systems; however, performance data from the telemetry indicates that the condition of the system has degraded considerably.

2.2.7 Objective

Demonstrate the ability of the payload Doppler and Command system to operate payload equipment as commanded.

Objective Achieved

The Doppler and Command system has received and operated satisfactorily on commands from Manchester and Hawaii.

2.2.8 Objective

Determine performance of the payload data system. This consists of the 378.21-mc telemetry transmitter, the digital instrumentation system, and the experiment sensors.

Objective Achieved

The payload data system is returning performance data and experimental results over interplanetary distances in a satisfactory manner.

2.2.9 Objective

Continue evaluation of the Stage I airframe, propulsion, and modified autopilot control systems.

Objective Achieved

Performance of the Thor booster was satisfactory in all respects.

3. PRELAUNCH AND LAUNCH TESTING

3.1 Prelaunch Testing and Simulated Countdown

The prelaunch testing of the THOR ABLE-4 second stage and payload started at the Los Angeles complex of the Space Technology Laboratories where comprehensive tests are performed on each stage prior to shipment to Cape Canaveral. The preshipment testing consists of a series of subsystem tests to determine the proper operation of each component and the performance parameters that might be expected. These tests were followed by integrated system tests during which all systems are operated under simulated flight conditions. The Thor No. 219 booster stage received a similar series of tests by Douglas Aircraft Company.

After the equipment was received at AFMTC, the system tests were repeated to determine that their operational ability was not affected during transit. The tests fall into two major groups: "covers off" and "covers on". In performing the covers-off test, all systems are operated in their proper sequence with the propulsion system valve sequencing done by pneumatic pressure as is the case in flight. This test is run on external missile electrical power with the umbilical connected so that functions may be monitored by direct wire. The covers on test is performed with the propulsion sequence simulated and with no pressure in the system. For this test the umbilical cord is removed and internal flight-type batteries are used. Data may be obtained during this test by telemetry and visual inspection only.

When the missile is erected on the launch stand a similar series of tests is performed that culminate in an integrated acceptance test which includes the operation of each stage and the payload. This test is similar to the covers off test with the exception that the propulsion system is simulated.

3.2 Launch

On 29 February, T-8 day, the Able Stage II was removed from Hangar AA, towed to Complex 17A and mounted on the Thor 219 Stage I booster vehicle (Figure 3-1). The installation was completed in a routine fashion at 1410 hours. Umbilical ejection tests were performed the next day. The electrical ejection appeared sluggish, although the mechanical ejection performed satisfactorily. The electrical ejection trouble was traced to binding of the connector pins; realignment of the connector resulted in smooth, consistent ejection.

During tests on the second of March (T-6) imperfections were noted on the convergent section of the Stage III engine. Close inspection raised doubts as to the integrity of the stage. Due to the approaching launch date, a decision was made to recondition the year-old Stage III that had served as a back-up unit for THOR ABLE-3. The older backup stage was brought out and reconditioning proceeded. A resistance check was made and the old motor was found to be exactly within tolerance. The weight of the old stage was found to be slightly heavier than the stage originally scheduled to be flown; however, it was decided that this slight increase in weight would have no adverse effect on the over-all performance of the flight.

On the fourth of March, T-4, the Stage III was hoisted to the gantry and installed on the Stage II (Figure 3-2). The interstage fan assemblies were installed, but alignment proceedings were postponed because of high winds.

During the morning of the seventh of March, bonding and pinning of the third stage III/IV interstage structure to the third stage was completed, and the alignment was completed satisfactorily. The S/N 2 payload was installed (Figure 3-3) and the first "on stand" integrated payload test was completed without incident. The first day, T-2, the four solar paddles were installed on the payload (Figure 3-4) and tested. The paddles performed according to specification.

Figure 3-1. Able Second Stage Being Mounted on First Stage Booster Vehicle.

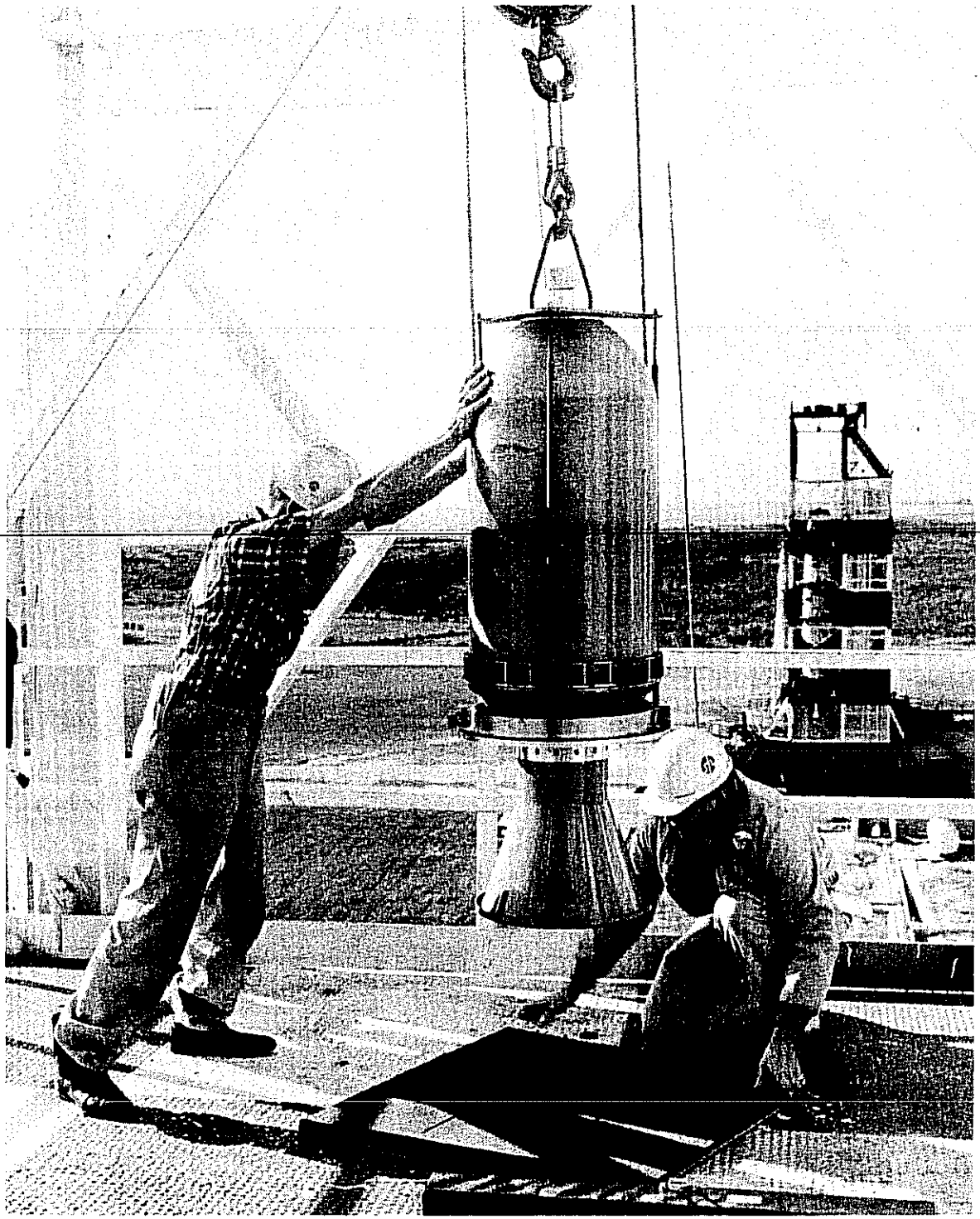

Figure 3-2. Third Stage Installation.

Figure 3-3. Installation of Payload on Third Stage.

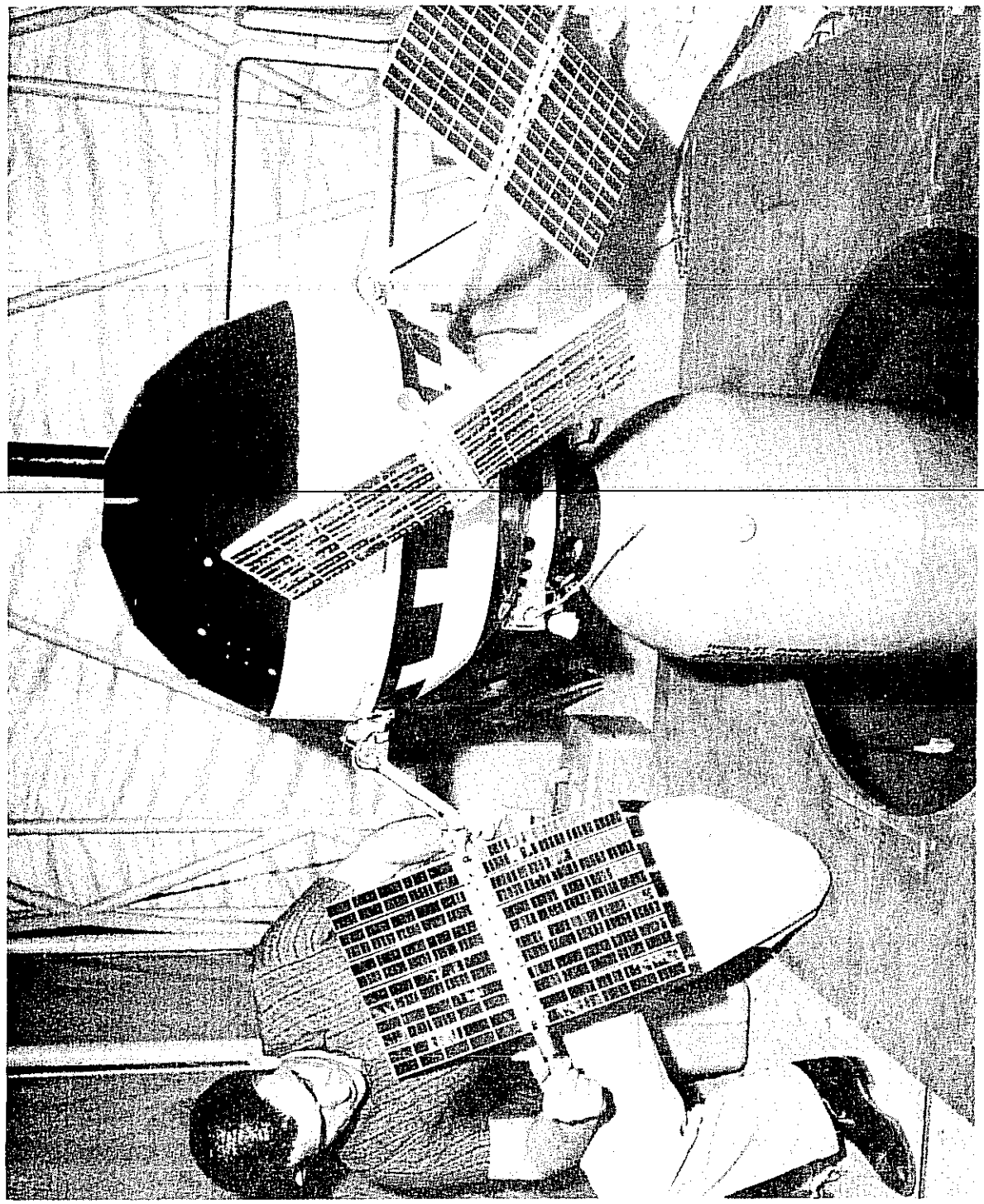

Figure 3-4. Installation of Solar Paddles on Payload.

Early in the morning, T-1, the precount tasks were begun with the payload acceptance test, followed by the sequence guidance and link loop tests. These tasks were completed in good order and the telemetry flight battery was installed in the Stage II. The fueling of the Thor booster vehicle began and the area was declared "Red". Stage II servicing was completed by Aerojet-General personnel and a fuel watch was set up until removal of the gantry.

T-0, the countdown continued at midnight, with all stations reporting to the Able Director. The final solar cell electrical checks and ordnance tasks were checked off as completed. The gantry was removed 20 minutes behind schedule.

During the late portion of the scheduled T-35 minute hold, a leak developed in the line between lox storage tanks and the lox topping tanks in the Douglas complex. Vigorous efforts were made to repair the malfunction while the countdown continued. At T-38 seconds, "No-Go" was announced by the lox topping crew. The supply in the topping tanks was depleted and could not be replenished in time to launch within the allowable time period. Condition III was announced at 0825 hours.

The operation abort invalidated all the tasks accomplished during the day. The launch was rescheduled for 0800 hours EST, Friday, 11 March.

The rescheduled launch countdown was initiated at 0300 hours EST, March 11. Final mission preparations, including ordnance provisions were completed at approximately 0430 hours. Light rain fell intermittently during the night and into the early morning hours, however, the prediction of fair weather proved to be correct. At launch the following climatic conditions prevailed: Temperature 57 to 64°F, relative humidity 93 percent, surface wind NNW at 11 knots, cloud cover 0.3 to 0.4 cumulus, 3200-foot ceiling with a secondary of cumulo stratus.

The final tasks, AGS guidance and payload check were completed at approximately 0540 hours (Figure 3-5). The scheduled one-hour hold was

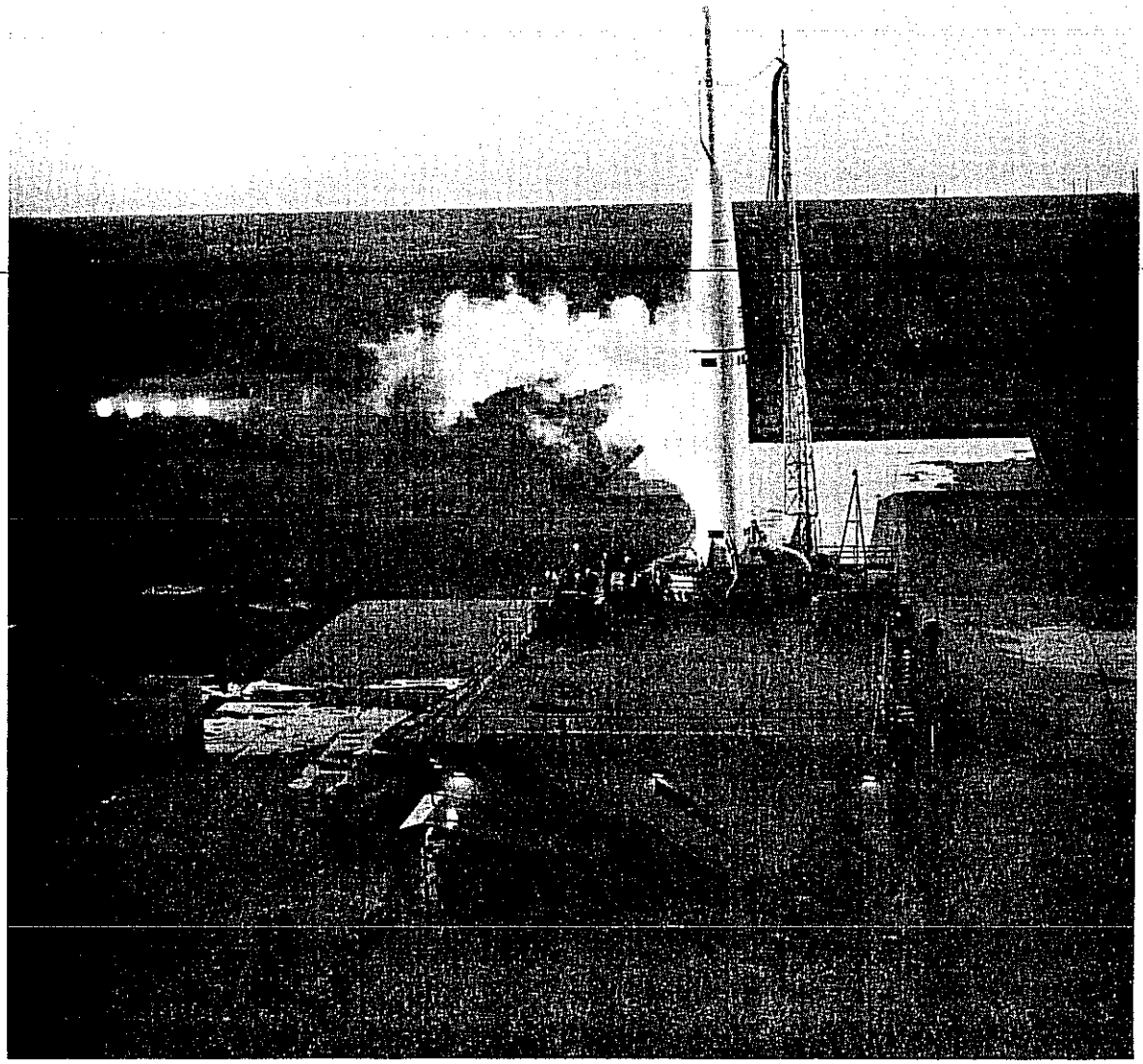

Figure 3-5. Final Launch Preparations.

executed at 0625 hours. A time sync was made as terminal count resumed at T-35, 0725:30 EST. The blockhouse was secured at 0736 hours. At T-27 minutes, pad safety declared the launch area clear.

T-6 minutes, blockhouse vents were closed. At T-50 seconds lox level was declared "OK". The count was perfectly on schedule. T-0, the ascent was smooth and positive. In a matter of seconds the THOR ABLE-4 vehicle had thundered into the scattered cloud cover at 4,000 feet. Lift-off occurred at 0800:06.99 EST from an original azimuth orientation of 90 degrees true. Gross weight at lift-off was approximately 113,511 pounds.

4 VEHICLE OPERATION

Reconstruction of the ABLE-4 powered flight trajectory provided data for propulsion system performance for each stage and the magnitude of attitude tipoff between the Stages II and III.

Stage I burnout conditions were used as a beginning for Stage II reconstruction, which consisted of simulating the actual commands sent by the guidance system during flight. The above procedure was followed in order to obtain values for the vehicle attitude at Stage II burnout.

Orbital parameters, determined from ephemeris data, were used as a basis for matching the powered flight trajectory to parameters specified to exist at 336 seconds after lift-off. Variations in the values of pitch and yaw tipoff (during the 3-second coast period after SECO), and specific impulse of the rocket engine during boost, were made to the assumed nominal parameters and dispersed trajectories were computed. Partial derivatives were evaluated from the above results. Appropriate changes to the missile parameters were calculated, which would cause the orbital parameters of the trajectory to converge to the values specified to exist at 336 seconds. Convergences were made for inertial velocity, azimuth, and velocity angle. The convergence was achieved with the following variations:

Stage II Burnout Conditions Following SECO

Attitude Tipoff	0.45 degree nose right 6.74 degrees nose down
Specific Impulse	1.1 percent above expected

	Actual	Expected
Radius From Earth's Center (ft)	21,912,784	21,874,735
Inertial Velocity (ft/sec)	25,617	25,565
Inertial Velocity Angle (deg)	75.405	74.83
Time of SECO (sec)	280.18	281.0

Stage III Burnout Conditions

Attitude Tipoff . . . . . 6.34 degrees nose down
Specific Impulse . . . . . 0.27 percent below expected

Based on an error analysis of the trajectory reconstruction, the error in the tipoff angle existing at Stage II burnout should be no greater than 0.5 degree. Therefore, it appears that the tipoff imparted to the third stage should have been on the order of 5.84 to 6.84 degrees.

The measured chamber pressure just prior to oxidizer valve closure was approximately the same as the value recorded during the fuel exhaustion shutdown of ABLE-3. From the above discussion, it is concluded that the chamber pressure decay, prior to THOR ABLE-4 SECO, resulted from fuel depletion. Although shutdown was initiated by guidance command, fuel exhaustion apparently occurred almost simultaneously.

Calculations, as discussed in paragraph 4.3.2, indicate that a continuous counterclockwise roll torque of approximately 1.6 lb/ft was applied to the second stage throughout the thrust duration period. The counterclockwise roll was initiated immediately after ignition and was not relieved until engine cutoff, when it diminished to zero. This indicates that the roll torque disturbance was initiated by the propulsion system. An investigation to determine the cause of the roll torque is being conducted.

4.1 In-Flight Events

Table 4-1 lists the sequence of events in the ABLE-4 launch operation with the nominal and recorded times from lift-off.

Table 4-1. Sequence of Events.

Event	Flight Value	Nominal
1. Lift-off (0800:6.993)	0	0
2. Start Thor Roll Program	2.5	2
3. Stop Roll Program (Stage I)	10.25	9
4. Start Pitch Program (Stage I)	10	10
5. Stop Pitch Program	140.60	140
6. Arm Second Stage	139.42	145
7. MECO	163.89	164.36
8. Stage II Ignition	165.93	166.9
9. Ignite Stage I/II Separation Bolts	166.28	166.9
10. Ignite HGA	176.00	176.9
11. Nose Fairing Ignition	185.48	191
12. Nose Fairing Separation	185.50	191
13. Command Yaw Left Start	204.80	
14. Command Pitch Down Start	206.28	
15. Command Yaw Left Start	217.91	
16. Command Yaw Stop Start	227.88	
17. Command Pitch Up Start	233.11	
18. Command Pitch Stop	239.41	
19. Command Yaw Right Start	242.02	
20. Command Pitch Down Start	253.03	
21. Command Yaw Stop Start	254.607	
22. Command Pitch Down Start	266.67	

Table 4-1. Sequence of Events (Continued)

Event	Flight Value	Nominal
23. Command Yaw Stop Start	272.97	
24. Command Pitch Stop Start	274.53	
25. Command Shutdown (Stage II)	280.18	281
26. Spin Initiation (Stage III)	282.17	283
27. Stage III Ignition	283.07	284.1
28. Strut Release (II/III Separation)	283.10	
29. Stage III Burnout	322.031	322

4.2 Stage Operation

Performance of the first stage, Thor Missile 219, was essentially nominal. The flight path of the first stage nearly duplicated the nominal preflight predicted trajectory. Main engine cutoff (MECO) occurred 1.43 seconds earlier than predicted, with a radial velocity with respect to the launch pad that was 260 ft/sec higher than predicted. The velocity vector at MECO was 1.0 degree high and 0.2 degree left of the nominal velocity vector, which was within the 6-degree half cone angle requirement. Lift-off weight was 113,511 pounds compared to an expected weight of 114,198 pounds. Vernier engine solo operation was normal.

4.2.1 Propulsion System

The propulsion system performance was excellent. Lift-off occurred 3.69 seconds after engine start command. Total engine thrust, computed from chamber pressure data five seconds after lift-off, was 153,400 pounds. MECO occurred at 163.89 seconds by actuation of the fuel injector pressure switches, which was 1.43 seconds earlier than predicted.

A propellant utilization of 99.8 percent was obtained from float switch and differential pressure data indicating liquid oxygen depletion at MECO with 100 pounds of impulse fuel available. The nominal propellant utilization expected was 99.5 percent. Vernier engine solo, subsequent to main engine operation, was 12.1 seconds.

Missile 219 was loaded with RJ-1 fuel and liquid oxygen. The use of the higher density RJ-1 fuel in the standard Rocketdyne MB-1 engine system provides a slight increase in the burning time, with a resultant increase in the total impulse and final velocity at MECO.

Key propulsion parameters are as follows:

	Actual	Expected
Main Engine Thrust at Sea Level, (lb)	151,100	152,035
Main Engine Thrust in Vacuum, (lb)	174,300	175,000
Main Engine Burning Time, (sec)	163.89	164.36
Mixture Ratio, Over-all (Avg)		2.07
Specific Impulse, Sea Level, Over-all (sec)	~243.72	249.2
Specific Impulse, Vacuum, Over-all (sec)	~282.43	288.9
Residual Propellants at MECO (percent)	0.2	0.5

4.2.2 Control System

The control system performance was satisfactory throughout Stage I boost. The near nominal flight trajectory indicates that the gyro drift, programmer timing, and inverter voltage were within the expected tolerances. Irregular low amplitude oscillations (10 to 14 cps) in pitch and yaw occurred at approximately 75.0 seconds in the region of maximum aerodynamic loads. The disturbance was damped to zero within 15 seconds. Pitch and yaw rate changes occurring at approximately 108 seconds

resulted from transients caused by autopilot gain change programmed to occur at 108 seconds.

The main engine shutdown and staging transients were of small magnitude. Approximately 0.8 second after MECO occurred, the Thor pitched down at 0.42 deg/sec and yawed right at 0.26 deg/sec.

4.2.3 Electrical System

Programmer roll and pitch commands were initiated according to specification. The main engine cutoff circuitry satisfactorily armed and initiated cutoff by actuation of the fuel injector pressure switches. The ac and dc voltages appeared normal throughout the flight.

All instrumentation systems functioned and provided adequate data with the exception of the turbine inlet temperature which experienced a dropout during the period from 72 to 74 seconds. No loss of data resulted from the telemetry signal disturbance during the period from 134 to 168 seconds.

4.2.4 Trajectory Analysis

The flight path of the first stage essentially duplicated the normal trajectory. Main engine cutoff occurred 1.43 seconds earlier than predicted with a velocity at MECO which was approximately 260 ft/sec higher than predicted. FPS-16 radar tracking data indicated a velocity with respect to the launcher (v_a) of 15,344 ft/sec at MECO. The nominal burnout velocity was 15,369 ft/sec based upon the preflight trajectory.

The velocity vector at MECO was approximately 1.0 degree high and 0.2 degree North of the nominal velocity vector.

Key trajectory parameters at 162 seconds* are as follows:

*No velocity and acceleration data was recorded beyond 162 seconds

	Actual	Expected	Error (A-E)
Velocity, Pad Reference (ft/sec)	14,620	14,460	160
Velocity angle from vertical (deg)	68.50	69.47	-0.97
Downrange Distance (ft)	531,300	528,045	3,255
Crossrange Distance (ft)	-1640	-2761	1,121
Geodetic Vertical (ft)	291,253	281,925	9,328
Azimuth of velocity vector (deg)	88.5	88.4	0.1

4.3 Stage II Operation

4.3.1 Propulsion System

The second stage was boosted by an Aerojet-General AJ10-101A propulsion system. The fire signal ignited the Stage II engine at 165.93 seconds after lift-off, with the shutdown signal from ground command initiated 114.25 seconds later. Steady-state operation was satisfactory with an average chamber pressure of 204.5 psia and an average thrust of 7645 pounds. The total impulse was 871,240 lb-sec. The average specific impulse was 266 lb-sec/lb.

The propellants loaded consisted of 2485.5 pounds of oxidizer (62°F at a S.G. of 1513) and 860.9 pounds of fuel (64.5°F at a S.G. of 0.790). The average propellant flow rates (based on static test parameters and in-flight chamber pressure data) were 21.25 lb/sec of oxidizer and 7.52 lb/sec of fuel which resulted in an average mixture ratio of 2.83. The total propellants consumed was approximately 3270 pounds.

The helium supply pressure was 1640 psia 10 seconds prior to lift-off. Ignition of the heat generator occurred 9.75 seconds after TPS actuation. Initial regulator pressure was 351 psia after Stage II ignition, decreasing to 308 psia at shutdown command.

Analysis of the recorded helium regulator pressure and chamber pressure data indicated that the chamber pressure data was invalid during the last few seconds of powered flight. The pressure transducer line was

restricted and did not sense chamber pressure. In order to determine the chamber pressure during the above period, two equations based on engine static test data and in-flight pressure data were equated. A comparison of measured and calculated chamber pressure data indicated that the in-flight chamber pressure was below the normal profile for a typical command shutdown.

4.3.2 Control System

Operation of the Stage II control system was considered satisfactory. However, control of the Stage II was complicated by three significant deviations from normal performance during the period of engine operation. The abnormal conditions are as follows: a) Roll attitude offset greater than 2 degrees CCW; b) engine misalignment in pitch was excessive at 0.65 degree pitchup; and c) large body rates, 1.8 deg/sec pitch-down and 0.4 deg/sec yaw-right, were developed during engine shutdown and existed after shutdown.

The Stage II gyros were uncaged simultaneously with the engine fire command at 165.9 seconds. Approximately 0.5 second after Stage II ignition, the missile rolled CCW at about 1.64 deg/sec, with the CW control jet operating at a 2 degree CCW attitude. A limit cycle was established of about $\pm$0.3 degree centered on 2.5 degrees CCW, with a period of 2 seconds. The parabolic roll attitude divergence indicated that a net roll torque of 1.6 lb-ft was applied to the missile. Following the first CW roll jet operation, the missile roll attitude limit cycled for an average period of 2.1 seconds with an amplitude of $\pm$0.3 degree centered on 2.5 degrees CCW. During the operation of Stage II, the CW roll control jet operated a total of 59 times for a total roll jet on time of 9.13 seconds out of the 124.2 seconds engine operating time.

An analysis of the Stage II roll control system was performed to establish that the performance of the system agreed with the flight dynamics when an external roll torque of 1.6 ft/lb was applied to the

system. The analysis confirmed that the average period and average on-time per cycle agree with the applied roll torque value.

Two independent computations were made to establish the magnitude of the roll torque which operated on Stage II throughout engine burning. The roll gyro returned to zero at engine shutdown indicating that the roll torque applied to the system vanished when the propulsion system shut down. The only possible source of this roll torque, other than the propulsion system, is a roll torque produced by a leak in the CCW roll control jet. Had this been the case, a larger utilization of helium would have occurred than was indicated by telemetry data. The roll torque experienced on the THOR ABLE-4 flight was approximately three times the roll experienced on previous ABLE flights. The external roll torque does not appear to correlate with other system errors such as pitch and yaw engine misalignment. Therefore, it is concluded that the roll torque was applied by the propulsion system.

Body rates of approximately 1.8 deg/sec pitch-down and 0.4 deg/sec yaw-right were recorded at SECO. Two possible causes of the attitude rate error have been considered: a) angular rates resulting from interruption of fluid flow (valve closure) at SECO, and b) transient caused by changes in engine misalignment with thrust removal at SECO. This is discussed in detail in Section 4.4.

4.3.3 Advanced Guidance System

The over-all performance of the closed loop consisting of the Advanced Guidance System, computer, autopilot, and missile, resulted in satisfactory burnout conditions. The only two significant sources of error in the trajectory were contributed by the discontinuity of attitude between Stages II and III (see paragraph 4.4) and the improper resolution of the AGS fine measurements of p and q.

Because of difficulties in the 4.0-mc position-measuring subsystem, this ambiguity resolving subcarrier was not planned for use on the THOR ABLE-4 flight. Only the fine p and q measurements were used, and

the integer number of wave lengths for the interferometric position-measuring system was determined by up-dating the last p with p-dot starting with a fixed p and q corresponding to the launch pad.

The inherent difficulty in determining p and q by this method is that, after a period of noisy data or data dropout, an improper resolution of the integer number of wave lengths may be made, resulting in gross errors in p and q.

4.3.3.1 Noise in AGS Data

The noise in the AGS outputs has been defined as the rms difference between raw data and data smoothed over 10 or 20 points. The data smoothing was accomplished by passing the raw data through a third-degree polynomial filter with a cutoff frequency of 0.25 cycle/sec. The observed noise in the r-dot, p-dot and q-dot is as follows:

a) At lift-off, the noise in r-dot was approximately 0.13 ft/sec, which is normal, and it increased steadily for about a 20-second period. After this period, the noise decreased to a minimum of 0.11 ft/sec at about 55 seconds, after which it again rose to a value of approximately 1.1 ft/sec near the end of the Thor stage. During Stage II operation, the r-dot noise increased from 0.14 to approximately 0.6 ft/sec at cutoff.

b) The noise in p-dot increased from 0.07 to 0.22 ft/sec shortly after lift-off and then decreased to approximately 0.25 ft/sec at about 60 seconds from lift-off. The noise remained at approximately this low level until missile flame attenuation, which caused a 15-second period of data dropout. Just prior to the dropout, the noise increased sharply and remained high until system lock was regained, at which time the noise decreased to 0.01 ft/sec and remained at this level until Stage II burnout.

c) The q-dot noise increased from 0.07 to 0.165 ft/sec shortly after lift-off, and decreased to 0.025 ft/sec at about 60 seconds after lift-off. The noise remained at this level until the dropout and returned to a level of 0.06 ft/sec when system lock was regained. It remained at this level throughout the rest of Stage II operation, except for a 15-second increase to 0.95 ft/sec at about 210 seconds after lift-off.

4.3.3.2 Ambiguity Resolution

It has been determined that a total error of three wave lengths in q and one wavelength in p were made. One wavelength in q was lost at lift-off, and two more in bridging the 17-second drop during the latter part of THOR operation. One wavelength in p was lost shortly after the 17-second dropout. Except for the one wavelength at lift-off, these integer resolution errors would probably have been avoided by using narrower gates. The gate may be defined as the maximum permissible noise in the second difference of rate data. When the noise in the rate data causes the second difference to exceed the fixed gate size, the computer edits the data by rejecting the point.

On THOR ABLE-4 the second differences in p-dot and q-dot before the dropout were 0.05 and 0.8 while the errors were on the order of 0.2 and 0.5 ft/sec, respectively. While the probability of bridging a 17-second data dropout without at least one wavelength error is low, even with a narrow gate, the smaller the gate the higher the probability of success; therefore, the gate should be set as low as noise will allow.

4.3.3.3 Steering

All six possible steering commands were sent and the missile appears to have responded correctly to all. A total of six commands in yaw and six commands in pitch were sent for a total duration of 18 seconds or a duty cycle of about 17 percent. The attitude error of the vehicle at SECO was computed in real time to be -2 milliradians in yaw and -15

milliradians in pitch. The actual attitude errors at SECO were determined by correcting the wavelength errors in the AGS data, computing raw attitude errors, and then filtering, with the assumption that the missile turned at the commanded rates. The errors at SECO computed by this method were 4 milliradians in yaw and 46 milliradians in pitch. However, the q-dot noise makes the pitch attitude error at SECO subject to a 20 milliradian uncertainty.

There was a 0.5 ft/sec error in q-dot at approximately 210 seconds after lift-off which passed the 1 ft/sec gate and caused raw attitude errors of 16 radians in pitch and -7 radians in yaw. This transient would not have passed the gate if the gate size was less than 0.5 ft/sec, or if the point had been followed by good data. The result of the transient was an undesirable pitch-up command and an over-correction in yaw.

4.3.4 Electrical and Sequencing Systems

The Stage II electrical and sequencing systems functioned as designed.

4.3.4.1 Electrical System

Performance of the prime power battery was satisfactory. Battery voltage just prior to launch decreased to 27 volts dc then rose to 28 volts dc at lift-off. The voltage was initially one volt lower than expected due to the 50°F ambient temperature of the battery which was on the low side. As the battery discharges, the internal temperature rapidly rises to restore the voltage to the normal value of 28 volts minimum. The telemetered nominal 25.5 voltage trace drifted out of calibration, compared to the 28.3 volts dc noted on the launch console at lift-off.

4.3.4.2 Sequencing System

The in-flight sequence of events functioned satisfactorily. The time-delay relay which initiated Stage III ignition completed its function in 2.89 seconds instead of 3.1 seconds as obtained in prelaunch testing.

However, the 6 percent decrease in time delay remains within the relay tolerance. The same relay on ABLE-3 demonstrated similar characteristics.

4.4 Stage II/III Separation

All staging events occurred at approximately the nominal time and Stages II and III satisfactorily separated. However, pitch and yaw rates initiated at SECO were prevalent at Stage II/III separation. Rates of 1.8 deg/sec pitch down and 0.4 deg/sec yaw-right were recorded at SECO. No instrumentation was provided to directly measure tipoff at stage separation. Consequently, it was necessary to determine tipoff information from control system measurements and trajectory data. The estimated attitude error after Stage II/III separation resulting from the error generated during the period from SECO through separation, and the attitude error from the pitch rate at separation is estimated to be 5.1 degrees pitch-down and 2.2 degrees yaw-right. Figure 4-1 is a plot of pitch, yaw and volt demodulator data at SECO and thrust chamber pressure for the same period. A post-flight reconstruction of the trajectory provided Stage II tipoff values of 6.74 degrees pitch-down and 2.2 degrees yaw-right. Similar angular rates have been observed on other flights with the AJ10-101 propulsion system and are tabulated in Table 4-2. The observed rates appear to be of a larger magnitude for a propellant exhaustion type shutdown than for a command type shutdown.

Two probable causes for the attitude rate error were considered:

a) Angular rates imparted to the vehicle when the fluid flow (fuel or oxidizer) is interrupted during the engine shutdown sequence.

b) Transient caused by changes in engine thrust alignment with thrust removal at shutdown.

The possibility that the pitch and yaw rates resulted from a sudden stoppage of the propellant flow caused by valve closure was investigated.

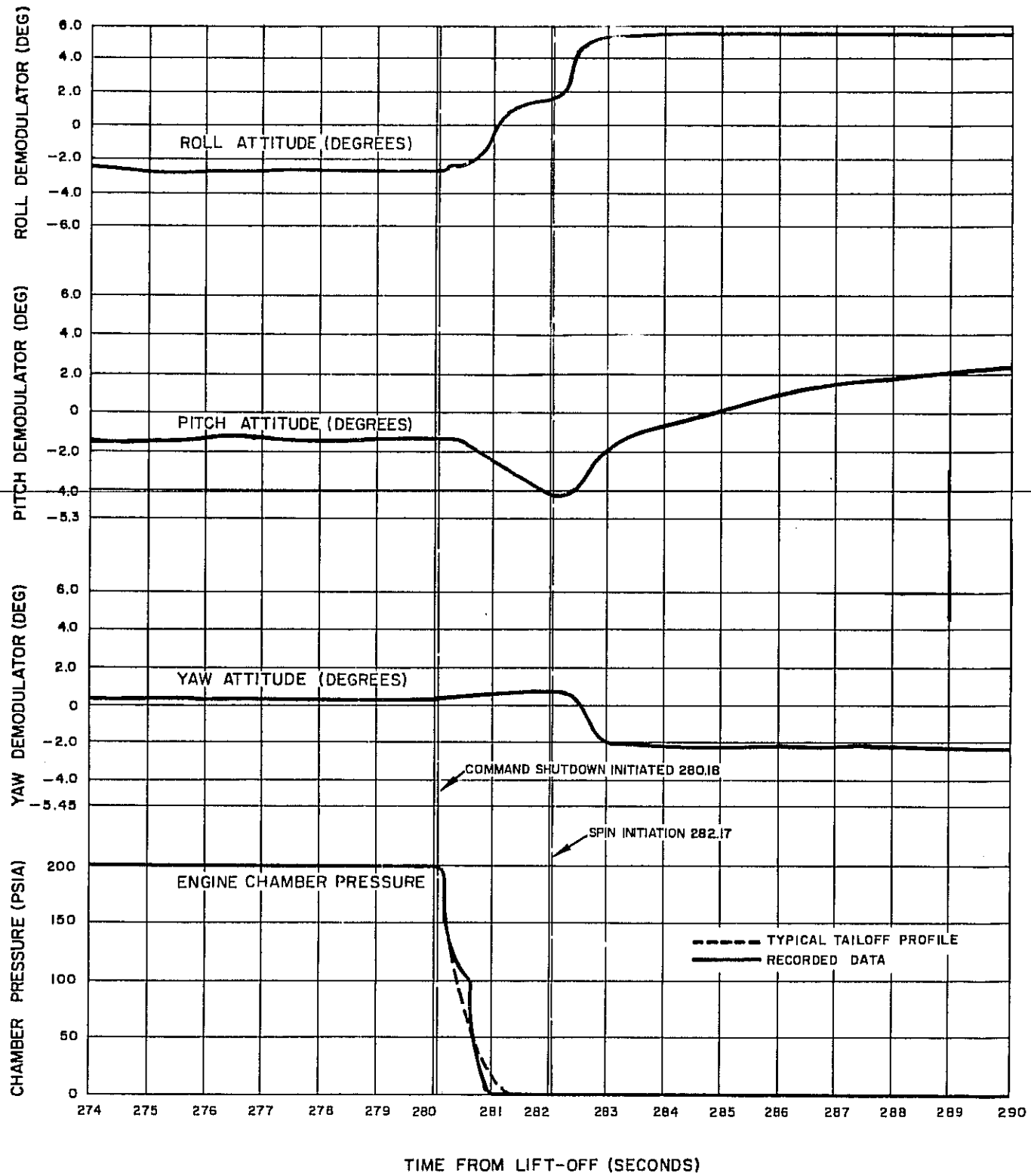

Figure 4-1. Missile Attitude and Thrust Chamber Pressure Versus Time.

Table 4-2. Summary of Attitude Errors for ABLE Second Stages.

Vehicle No.	Payload	Type of Shutdown	Shutdown* Time (Secs)	Burnout Pitch Rate (+ pitch up)	Burnout Yaw Rate (+ yaw rt)	Pitch** Engine Offset (+ pitch up)	Yaw** Engine Offset (+ yaw rt)	Roll Torque (ft-lb)
Thor 129	ABLE 1	Ground Command	Less Than 0.250	0	0	0	-0.25	0.067 CCW
Thor 130	ABLE 1	Acceler-ation Command	Less Than 0.250	0	0	-0.4	+0.15	0.225 CCW
Thor 132	ABLE 2	Ground Command	0.075	-0.2	0	-0.08	+0.48	0.5 CCW
Thor 133	ABLE 2	Ground Command	0.030	-0.2	-0.2	+0.1	+0.2	0.26 CCW
Thor 134	ABLE 3	Fuel TPS	1.0	-1.1	-0.8	-0.2	+0.3	0.065 CW
Thor 135	ABLE 2	Ground Command	0.100	+0.2	+0.1	-0.25	+0.55	0.16 CW
Thor 136	Transit 1A	Ground Command	0.040	0	0	-0.1	+0.4	0.27 CW
Thor 137	ABLE 2	Ground Command	Transducer Inoperative	+0.3	+0.2	-0.05	+0.4	Indeterm-inant CW
Thor 219	ABLE 4	Combined Fuel TPS & Ground Command	0.350	-1.8	+0.4	-0.65	+0.3	1.6 CCW

*Time from shutdown initiation to approximately 5% of running chamber pressure

**This reading is actually the steady-state demodulator offset divided by 2.0 (corresponding to $\delta/\theta = 0.5$)

Approximations were made of the angular impulse and resultant angular velocity produced by the valve closure, based on propellant line geometry and flow rates. From the above approximations, it was concluded that the angular impulse attributed to valve closing is too small and in the wrong direction to produce the attitude errors observed on ABLE-4.

In order to evaluate the effects of engine thrust misalignment on attitude errors, an analog computer study was performed. The computer study assumed system parameters equal to those of the pitch-yaw system of THOR ABLE-4 at Stage II burnout. A thrust misalignment was assumed to exist which was equal to zero degree for zero thrust and one degree for full thrust, analogous to the misalignment which would occur if the thrust structure was deformed elastically by thrust. In the course of the engine shutdown, this thrust-dependent misalignment would act as a disturbance to the attitude control system and the control system would attempt to control the vehicle to maintain zero turning rate. If the engine shutdown is extremely rapid, the resulting disturbance will be of small magnitude. If the engine shutdown is extremely slow, the attitude control system will be able to follow and remove the transient disturbance caused by the variation in engine misalignment. However, there exists a critical engine shutdown time where a substantial disturbance is introduced by the thrust dependent misalignment and where the control system does not have adequate time to remove this disturbance. In the latter case, a body attitude rate error will exist following engine shutdown. Figures 4-2 and 4-3 show the magnitude of the body rate at thrust termination as a function of the engine shutdown time.

For Figure 4-2 a thrust decay curve of exponential form was assumed. Results of the analog simulation indicate that a maximum body rate of 1.85 deg/sec is established when the time constant of the exponential thrust decay is equal to 0.25 deg/sec. Results in Figure 4-3 were obtained by assuming a linear thrust decay. In this case, a maximum body rate of 1.75 deg/sec was established when the decay time was equal to 0.8 second. Since neither thrust decay curve assumed represents

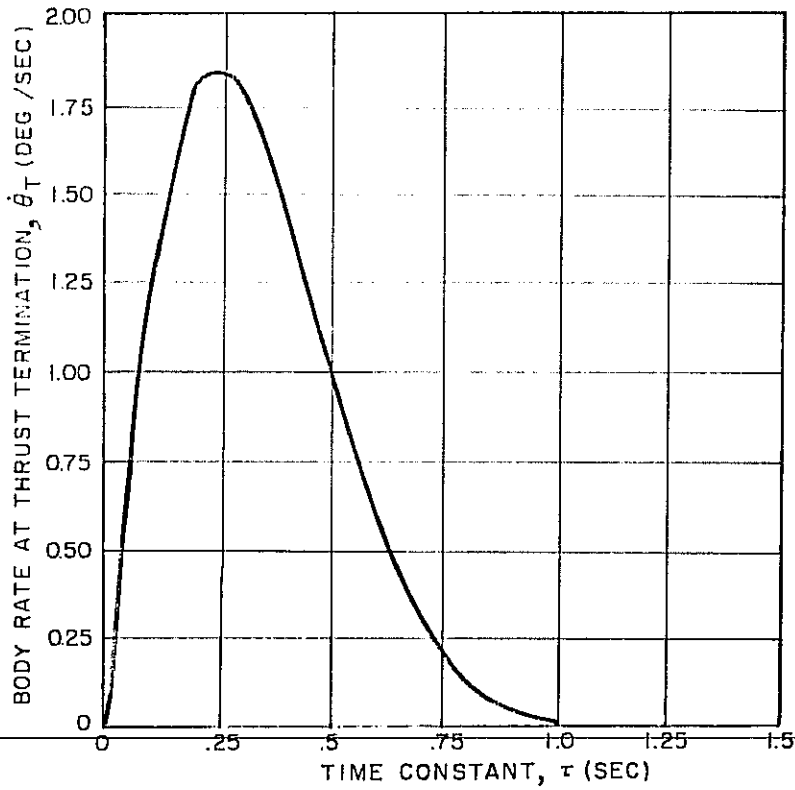

Figure 4-2. Body Rate Error at Thrust Termination (linear form) $T = T_o (1-t/\tau)$.

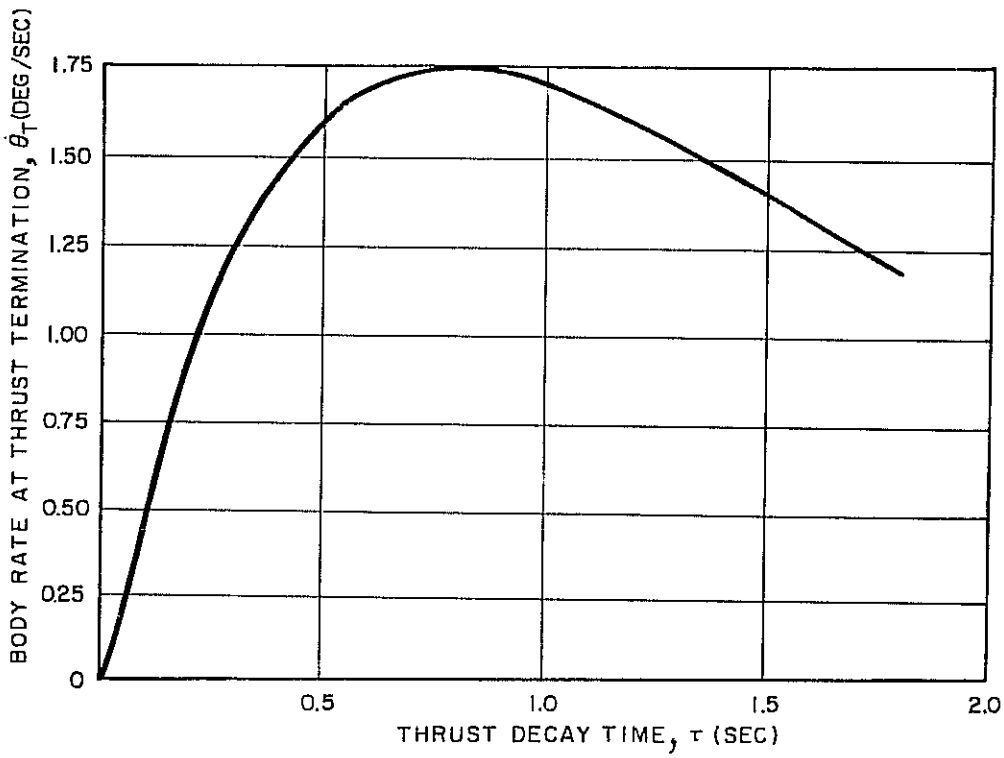

Figure 4-3. Body Rate Error at Thrust Termination (exponential form) $T = T_o e^{-t/\tau}$.

accurately the actual thrust decay characteristics, it can be concluded that body attitude rates of approximately 1.8 deg/sec can result from a one-degree engine misalignment linearly dependent upon thrust.

Flight test results for THOR ABLE-4 indicated that a misalignment of 0.65 degree pitch-down existed through Stage II flight. From the analytical investigations previously mentioned, it was concluded that a total thrust-sensitive misalignment of approximately one degree would be required in order to develop the observed 1.8 deg/sec pitch-down rate error. However, the sign of the thrust misalignment evidenced through flight and the body rate error developed at shutdown are opposite. If an engine misalignment is developed under thrust loading in the pitch-down direction, then the transient resulting when the thrust is removed will yield a pitch-up body attitude rate error. Therefore, if the rate error developed with the THOR ABLE-4 second stage is caused by thrust-sensitive misalignments, these misalignments are not responsible for the large engine misalignment evidenced throughout Stage II powered flight. A combination of thrust-sensitive misalignment and thrust-insensitive misalignment can be reasoned which is consistent with the observed results; however, the thrust-insensitive misalignment required is very much larger than 0.25 degree, the engine alignment specification.

A satisfactory explanation for both the body rate errors at burnout and the large engine misalignments during flight, as indicated above, has not been resolved at this time. Work is continuing to establish a conclusive explanation for the observed phenomena. Results of the nine flights shown in Table 4-2 tend to indicate that large body rate errors at burnout exist only in those flights where engine shutdown time is relatively large (ABLE-3 and -4). Other tabulated flights indicate small body rate errors. In all of these cases, rapid engine shutdown was achieved, such that any thrust dependent misalignment did not have sufficient time to create a large error.

4.5 Stage III Operation

4.5.1 Propulsion

The ABL X248 rocket motor used on Stage III of the ABLE-4 vehicle performed satisfactorily. Reconstruction of the powered-flight trajectory indicates that the total impulse of the engine was between 116,170 and 117,770 lb-sec, with the specific impulse between 255.3 and 258.8 lb-sec/lb.

The above values, based on the post-flight trajectory reconstruction, represent differences of 0.27 per cent low and 1.1 per cent high, respectively, from the expected value of 116,488 lb-sec. The variation in performance cannot be reconciled due to dispersions in guidance tracking data and rocket motor static test data. Alternative methods of determining Stage III engine performance were unsatisfactory due to noise and bias in the tracking data.

4.5.2 Spin Rate

Spin rate of the Stage III/Payload configuration, as determined by the modulation of payload strength signal, was 2.2 rps prior to Stage II/III separation, compared with 2.19 nominal and 2.4 rps about 13 minutes following separation. No signal strength information was available during Stage III burning. The increase in spin rate may result from internal gas forces in the Stage III rocket motor. A similar phenomenon has been observed in previous ABL X248 rocket motor firings.

A transient in the antenna pattern which was observed at Stage III/Payload separation was damped out in about 30 seconds. Due to the short duration of the transient, it is assumed that the transient pattern was caused by Stage III interference with the antenna pattern rather than by payload oscillation.

4.6 Payload Operation

4.6.1 Power Supply

The performance of the payload power supply (Figure 4-4) is considered satisfactory and within the design limitations of the system. The recorded battery temperature was higher than anticipated but remained within the design limits, although the efficiency of the system has been slightly reduced.

All four solar cell paddles appeared to function properly. The 4800 solar cells (1200 cells per paddle) were oriented to produce a nearly constant power output at an effective area between 22 and 25 percent. All paddles satisfactorily erected and locked in their intended position. Paddle number one with two temperature probes (an upper paddle) experienced a change in temperature from 24 to 64°F for the first 30 days after launch. The primary reason for the change in temperature is due to the reduction of the satellite's spin axis angle in reference to the sun angle which increases the exposure time of any one paddle to the sun. A less significant factor is the satellite's continuing movement toward the sun, thus being exposed to a higher ambient temperature.

The current generated by the photovoltaic energy converter is difficult to determine with any degree of accuracy due to the lack of solar cell current monitor. An approximation of 750 milliamperes has been calculated on the basis of battery voltage and charge time after a known discharge has been imposed.

The battery package of the payload power supply has supplied the needs of the scheduled interrogations. Consisting of 14 Sonotone nickel-cadmium Type F cells connected in series, which are connected in parallel with an identical pack, the battery provides a total capacity of 3.0 to 4.5 ampere-hours. The battery voltage is designed to be regulated between 14.8 and 21 volts dc; however, during interrogation the telemetered voltage may vary between 14.8 and 19 volts due to the loading by the transmitter.

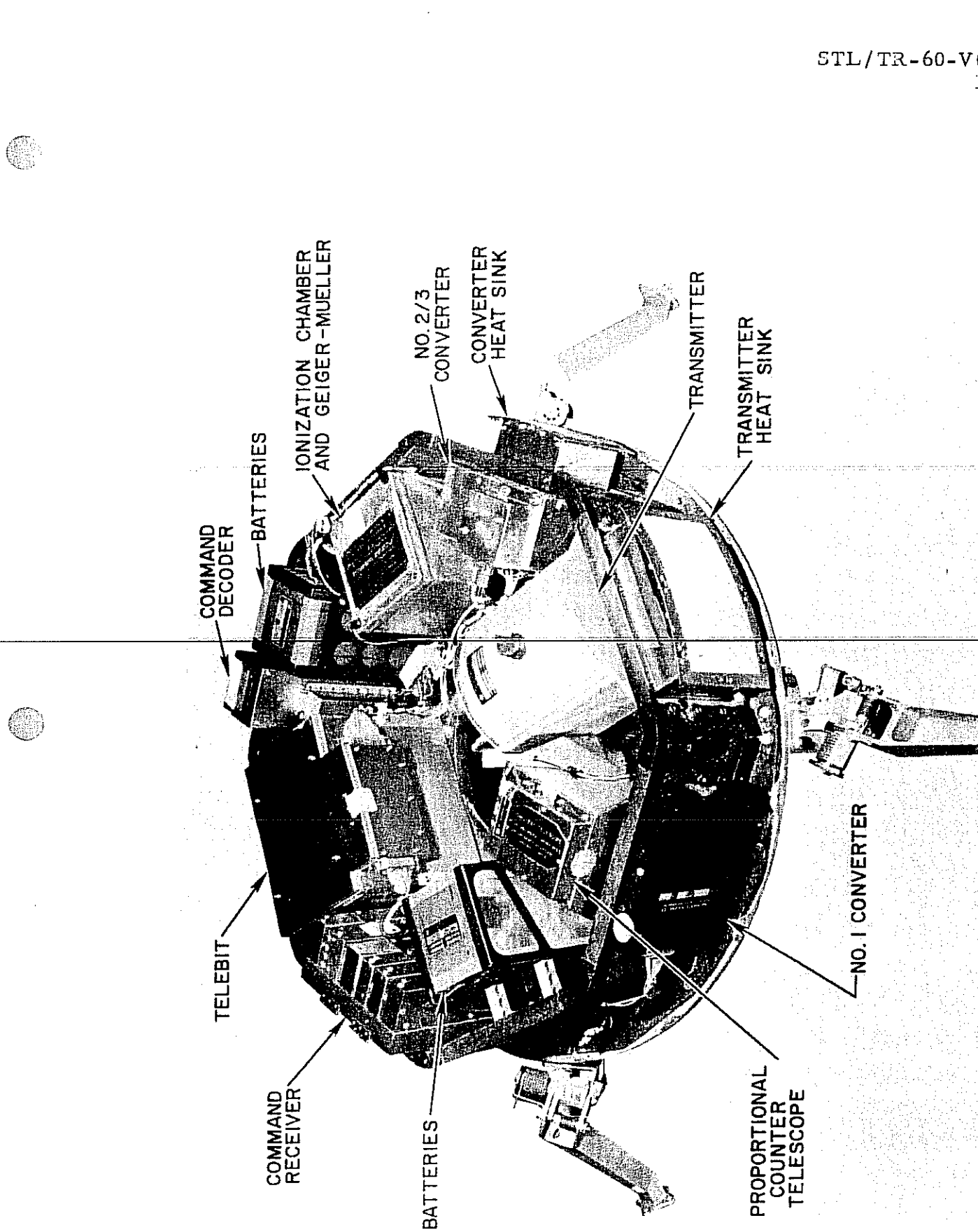

Figure 4-4. Payload Upper Shelf.

The battery as well as system voltage has been between 18.6 and 16.8 volts dc for a 20- to 30-minute discharge cycle. For periods of twice this duration a variation of from 18.6 to 15.5 volts has been noted. The accuracy of these readings is ± 0.5 volt and for a two-week period was as poor as ± 1.0 volt, when only odd digital numbers were recorded at the SpaN Center. A slight trend has been observed of a greater variation of battery voltage for a given interrogation period. Although sufficient data has not been recorded to substantiate any positive degradation, a possibility exists that because of higher solar cell paddle, battery, and load component temperatures, the system efficiency may be reduced to reflect more severe discharge on the payload batteries.

The payload batteries were expected to operate between 45 and 80°F; however, the telemetered temperatures have varied from 65°F after launch to 85°F after 30 days of operation with the exception of as high as 110°F immediately after a long overcharge period. This higher temperature reduces the battery efficiency 10 per cent and lowers the terminal voltage 5 per cent. Continual overcharge of the batteries, if maintained for an extended period of time at a temperature in excess of 107°F, will degrade and eventually destroy the batteries. This condition has not been experienced with the exception of one cycle to 110°F for a day when a malfunction occurred at one of the ground stations, which prevented the batteries from being discharged as per schedule.

The temperature protection backup consisting of four thermal switches (two paralleled per battery pack) which, when activated, insert a series resistor of 15 ohms between the battery and the solar cells, has not been activated. These switches have been set to activate at 120°F, at which time the solar cell charging rate is reduced in value to maintain the constant loads plus trickle charge the battery at the maximum solar light intensity.

Battery capacity has degraded during the lifetime of the payload such that it is only possible to operate the 5 watt transmitter for approximately 16 minutes during a single interrogation.

4.6.2 Radio Communication

The radio communication link with THOR ABLE-4 has performed successfully since launch. The payload transmitter was acquired six minutes after launch and was turned off by the Manchester ground station 25 minutes later. In subsequent weeks the transmitter has been operated on a duty cycle of about 10 per cent. For every hour of transmission time about 10 hours of battery recharging takes place.

The payload command receiver is a transistorized, double-conversion, phase-lock-loop receiver which produces a coherent output at 16/17 of the received frequency and has an operating capability with either a 250 or 40 cps bandwidth. The receiver operates continuously and, since its bandwidth is less than the frequency uncertainty of the received signal, repeatedly sweeps over a range of 40 kc searching for the carrier. When the receiver acquires and locks on a signal from the earth, the sweeping stops and the receiver can then accept any of the commands employed in the payload. On 16 March 1960, when the vehicle was at a distance of 4.2 million miles from earth, the command was sent to adopt the narrow-band mode of operation. As a result, the receiver will now search over a frequency range of 18 kc rather than 40 kc. The narrow-band command is irrevocable.

Another function of the receiver is to accept and process a CW signal from the ground, then provide the transmitter with a signal that is 16/17 of the received frequency; thus the transmitter will only operate while a CW signal is being received from the ground. The transmitter utilizes the 16/17 signal as the carrier frequency for information transmissions to the earth. A representative transmission log is presented in Table 4-3.

Table 4-3. Representative Transmission Log.

Date	Station	Time (Greenwich)	Range (naut mi)	Signal Strength (dbm)
3/11	Manchester	1335	7,025	-113
	Manchester	1535	29,919	-132
	Manchester	1635	35,200	-90
	Manchester	1835	50,700	-95
	Hawaii	2215	75,900	-121
	Hawaii	2345	84,600	-121
3/12	Hawaii	0230	100,900	-125
	Singapore	0501	117,000	-137
	Hawaii	0520	119,340	-124.5
	Singapore	0722	130,000	-138
	Singapore	1115	152,000	-139 to -140
	Manchester	1545	178,700	-114
	Manchester	1845	196,500	-115
	Hawaii	2245	218,000	-131
3/13	Singapore	0730	264,000	-144.5
	Manchester	1415	302,000	-116
	Manchester	1845	325,500	-120
	Hawaii	2236	346,000	-131
3/14	Hawaii	0130	359,200	-134.5
	Hawaii	0720	390,700	-137
	Manchester	1400	426,000	-119
	Manchester	1857	448,800	-120
	Hawaii	2245	480,400	-139
3/15	Hawaii	0730	514,500	-140
	Manchester	1430	550,200	-125
3/16	Hawaii	0735	636,000	-144
3/17	Hawaii	0735	755,700	-145
	Manchester	1430	790,200	-135

Table 4-3. Representative Transmission Log (Continued).

Date	Station	Time (Greenwich)	Range (naut mi)	Signal Strength (dbm)
3/18	Hawaii	0730	874,200	-139 to -148
	Manchester	1455	910,700	-133
3/19	Hawaii	2246	1,068,300	-149.5
3/20	Hawaii	0229	1,083,200	-151
	Manchester	1815	1,162,100	-138
3/21	Hawaii	0230	1,201,000	-148.5
	Manchester	1816	1,279,600	-138
	Hawaii	2246	1,300,300	-149
3/22	Hawaii	0231	1,315,500	-150
3/23	Hawaii	0700	1,457,800	-155
3/24	Hawaii	0146	1,546,100	-157
	Manchester	1702	1,622,000	-141

The THOR ABLE-4 payload is equipped with a five-watt transmitter (Figure 4-5) and a supplemental power amplifier. The power amplifier is used to increase the transmitter power from 5 to 150 watts as the distance of the vehicle from the earth becomes such that reception at the ground station becomes unreliable. The supplemental power amplifier was successfully turned on 8 May 1960 when the payload was at a distance of 8.2 million nautical miles.

The five-watt transmitter consumes 43 watts from the dc-to-dc power converter at various voltage levels and has the capability of operating continuously for two hours without discharging the batteries to the under-voltage cutoff point. When the supplemental power amplifier is used, however, the power consumption is raised to the point where transmission time must be reduced to five to eight minutes. When the change in transmission power level from 5 to 150 watts is made, a coaxial relay switch removed the five-watt transmitter output from the antenna, directing it into the power amplifier, and a second coaxial relay connects the power amplifier to the antenna.

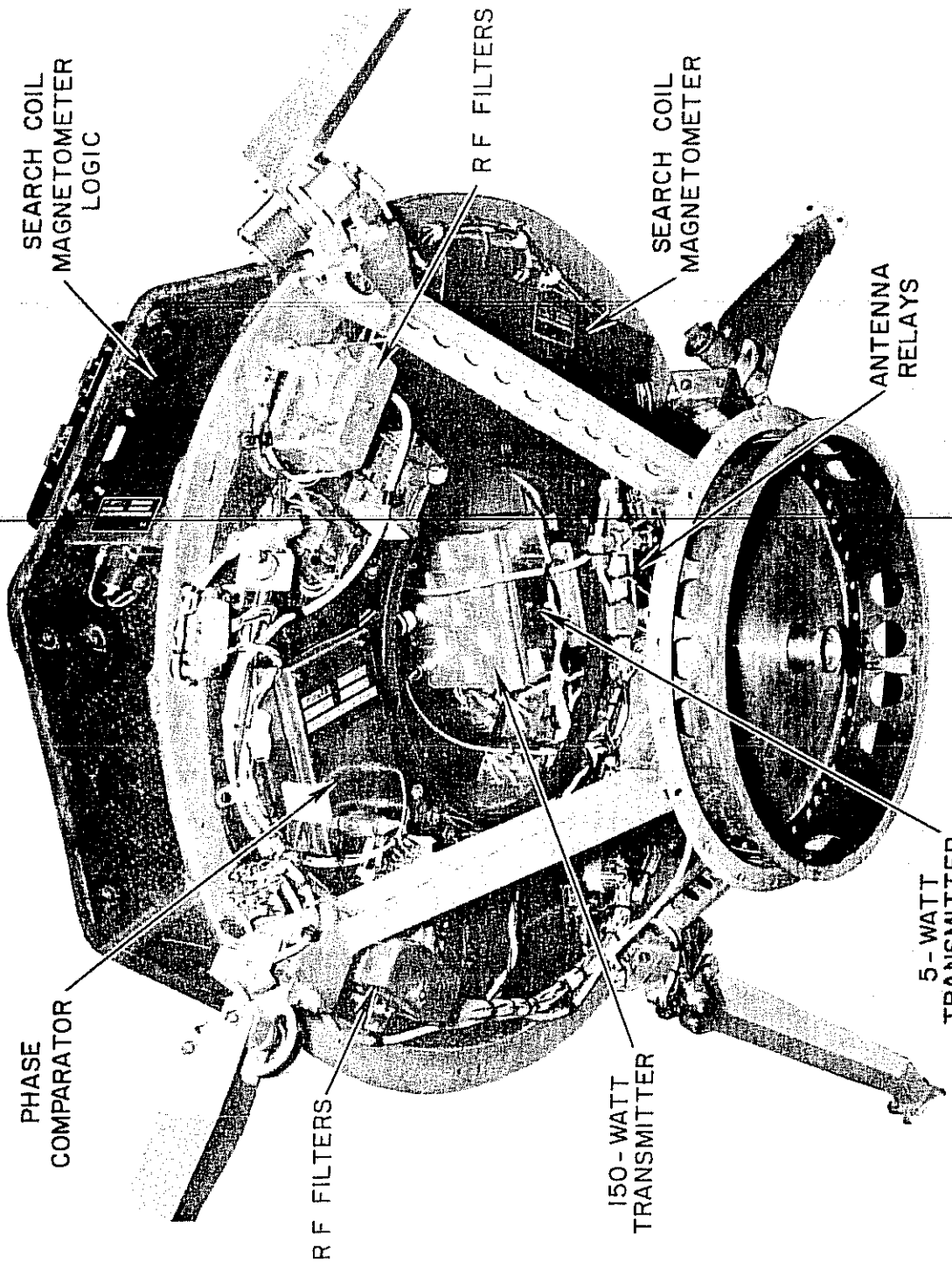

Figure 4-5. Payload Showing the 5- and 150-Watt Transmitters.

4.6.3 Digital Telemetry

Even though the primary mission of the THOR ABLE-4 space probe (Figure 4-6) was to gather scientific data, a second and highly important purpose of the vehicle was to serve as a test for various systems, such as the digital telemetry called Telebit. The function of the Telebit is to collect information in digital or analog form from the various experiments, store the information, and present it in the proper sequence for transmission to earth. The unit requires only about two watts of power for operation.

Corresponding to each of the seven information words (or numbers) that will be transmitted to earth is a register, called a shifting accumulator, which functions in either of two modes: a) as a binary counter, or b) as a shift register during readout time. This shifting accumulator consists of twelve transistorized flip-flops which are energized through diode gates either to count or to readout. Each pulse output from a digital experiment is applied directly to an accumulator while each continuous output from an analog experiment is applied to an analog-to-digital converter.

Since there are eight words (seven basic experiments plus one word for frame sync) in a complete frame, each shifting accumulator is sampled 1/8 of the time. During this sampled time, each accumulator fed by a digital experiment recirculates the binary number back into its input so that the readout is nondestructive. Thus, after readout, succeeding counts add to this last number. If there are no additional counts for a time, the last number will be retransmitted at succeeding readouts. When the accumulated number from the digital experiments reaches 1023, the next pulse will clear the counter to zero. Accumulating the total number rather than clearing the register to zero after each readout provides redundancy and thus prevents loss of information in case some transmissions are unsuccessful. Analog shifting accumulators, however, clear to zero after each readout since there is no significance in accumulating an analog measurement.

Figure 4-6. Thor Able-4 Payload.

The number in each accumulator is sequentially gated out by an 8-place ring commutator (one "ON" segment for each word) which commutates at the word rate. During this gate time, exactly twelve pulses shift out the binary data from each accumulator. Since only one accumulator is read out at a time, the outputs of all shifting accumulators are tied to a single line. The composite binary coded signal on this single conductor is then applied to the biphase modulator where it encodes the subcarrier. The phase of this subcarrier is shifted 180 degrees every time a "one" occurs in the binary coded output signal and no change of phase results at the time of a "zero". Since a "one" is represented by a pulse and a "zero" by no pulse, zeros are automatically encoded on the subcarrier when no register is being sampled, as is the case during the frame synchronization word. The biphase-modulated subcarrier is the output of the payload telemetry unit and phase modulates the five-watt transmitter.

Beginning with the telemetry analysis on 16 April, a recurring problem in interpretation of Word 7 in the Telebit frame occurred. This word includes the subcommutated values of eight sensors for the condition of the payload, e.g., battery voltage, battery temperature, paddle temperature, paddle temperatures, etc. These values suddenly became meaningless with, for example, a battery voltage level indicated to be much too low to operate the transmitter while at the same time the transmitter was operating.

A thorough analysis of the Word 7 readings over a period of five days uncovered the trouble. A single open diode in the Telebit unit altered the logic of the circuitry to produce the changed readings. Since a new but consistent logic had been created, a translation code was prepared by means of which the Word 7 values could again be interpreted correctly.

4.6.4 Payload Temperatures

The temperature control of the THOR ABLE-4 payload appears to be satisfactory. Temperature measurements are providing useful data

for further improvement and refinement of temperature control design. On the basis of the actual flight trajectory and an estimate of the final tip-off angle, payload interior temperatures appear to be within 5 to 10°F of their predicted values.

The temperature sensor labeled "internal ambient," located on the inner periphery of the electronic shelf, is shielded from the upper half of the payload shell and measures the approximate ambient temperature of the lower electronic shelf (see Figure 4-5).

The measure of the lower shelf ambient has provided an improved estimate of the differential between the upper and lower shelf regions over that obtained from Explorer IV data. The differential in THOR ABLE-4 is estimated to be about 40°F at the 30 degree sun look angle at launch (as compared with 30°F estimated for Explorer VI), and about 50°F at the 7 degree angle 30 days after launch. The predicted payload mean temperature corresponding to the actual flight trajectory and Stage III/IV tip-off estimate is 55°F at 30 days. The actual value estimated from payload measurements is 54°F, with an uncertainty of ±5°F (Table 4-4).

The converter and transmitter sensors are located on heat sinks which are directly exposed to space on the equator of the payload (see Figure 4-3). After launch the converter and transmitter sensors indicated 41 and 49°F, respectively, at the beginning of each transmission period compared to a predicted mean payload temperature of 43°F, (Table 4-4). After 30 days the temperatures are 48 to 54°F compared with the predicted value, 55°F. Thus, the converter and transmitter heat sink temperatures are a good measure of mean payload temperature.

On the basis of the battery sensor and payload temperature differential, the upper electronic shelf ambient was 63°F shortly after launch and 80°F at 30 days, compared to predicted values of 58 and 70°F, respectively. The higher measured temperatures are due to the higher temperature differential within the payload compared to that in Explorer VI.

Table 4-4. Temperature Measurements
(Beginning of Transmission).

	12 Hours After Launch (°F)	30 Days (°F)	°F/D. T. U* Word Count
Lower Shelf Ambient	18	26	±3
Paddle Sensor 1	21	48	±2
Paddle Sensor 2	25	51	±2
Converter Heat Sink	41	48	±2-3
Transmitter Heat Sink	49	54	±6
Battery	69	89	±3
Predicted Mean	43	55	
Predicted Sun Look Angle (including estimated tipoff)	28	7	
Upper-Lower Electronic Shelf-Temperature Differential	±20	±25	
Predicted Temp. Differential	±15	±15	
Predicted Maximum Upper-Shelf Temperature	70		
Probable Maximum Upper-Shelf Temperature	80		

*Digital Telemetry Units (See Section 4.6.3)

After five-watt transmission periods as long as 47 minutes, the lower shelf ambient and battery sensors have increased only 2 and 6°F, respectively, indicating that the payload is only slightly affected by step power dissipations.

The payload temperature data have been consistent and sensitive to changes. The effect and magnitude of increasing payload temperature with diminishing range to the sun, the effect of payload attitude and sun look angle on local temperatures and on temperature differential, and the effect of transient power dissipations have been clearly indicated by the data.

4.6.4.1 Converter and Transmitter Heat Sink Temperatures

Converter and transmitter heat sink operations are performing according to design. At the beginning of every transmission period since launch, the heat sink temperatures have cooled off to their nominal nonoperating level with the exception of those few periods of frequent, long, successive transmissions. In the latter instances the heat sink temperatures have not been hotter than 7°F above their nominal nonoperating level. It appears that 30-minute transmissions less than three hours apart raise the operating level about 5°F. Similarly, 15- to 30-minute transmissions in less than two hours will increase the temperature level approximately 5°F.

The increase of converter and transmitter heat sink temperatures during various transmittal periods are shown in Table 4-5.

Table 4-5. Temperature Increases During Transmission.

Sensor	Length of Transmission (minutes)				
	15	30	35	40	45
Converter Heat Sink, °F	4-5	9-14	14-20	17-22	22-28
Transmitter Heat Sink, °F	5	18	21-23	23-26	30-33

The converter heat sink temperature rises for 15- and 30-minute operations agree with environmental tests. No environmental temperatures are available for comparison with measured transmitter heat sink temperatures.

Transmission with the five-watt transmitter in excess of 40 minutes will result in unsafe converter conditions except at ambient temperatures below 60°F. Operation of the five-watt transmitter for 45 minutes or longer is unsafe at ambient temperatures above 45°F, and for 50 minutes at ambient temperatures above 30°F.

4.6.4.2 Battery Temperature

The nominal battery temperature at the start of each transmission period has risen from 69°F after launch to 89°F after 30 days. In that time, the mean payload temperature has gone up nearly 12°F as predicted, the additional increase in battery sensor temperature being due to the increase in temperature differential as the presently warm upper half of the payload where the battery is located turns toward the sun, and due to a possible increase in sensor-to-ambient temperature drop as indicated in environmental chamber tests.

4.6.4.3 Paddle Temperature

Two sensors are located inboard and outboard on the same side of one of the four solar cell paddles. Three hours after launch the paddle sensors reached equilibrium at 21 and 25°F, measured outboard and inboard, respectively. (The inboard sensor is being warmed by radiation from the payload.) The predicted paddle temperature was 18°F at a sun look angle of 28°, in fortuitous agreement with that measured, considering the uncertainty in material optical properties, local thermal gradients, etc.

After 30 days the paddle temperature has risen to 48-51°F primarily due to the increase in solar projected area of the paddle with decrease in sun look angle, and decreasing distance from the sun. These temperatures are approximately 13°F higher than predicted.

4.6.4.4 Reliability of Temperature Measurements

The quality of the temperature data has been most gratifying and useful in verifying the thermal environment in the payload. Even in the presence of some severe operating conditions, such as battery overheating and overcharge, long continuous transmitter and converter operation, long periods of transmitter OFF, frequent periods of transmitter ON and launch aerodynamic heating,* the transmitted temperature data has been consistent and presents no unexplainable behavior.

It is of interest to note that, during launch, the effects of aerodynamic heating were indicated (by all six payload temperature sensors) to a greater or lesser degree depending upon location, as could be predicted. A maximum increase of 19°F was measured in the vicinity of the payload equator where the farthest foreward "external" heat sink sensors were located. The temperatures recorded following launch indicate that the average thermal time constant for the bulk of the payload components to reach equilibrium is 9 hours, with the exception of the more massive battery, which took 12 hours. The solar paddles reached equilibrium in less than three hours after launch.

One problem that exists is the interpretation of the Digital Telemetry Unit Data. As indicated in Table 4-4, all temperature data has an accuracy of ± 2 to ± 6°F, depending on the temperature width digital word count interval. From March 12 to 20 the DTU count was all odd due to ground station difficulties. As a result, the temperatures either did not change or changed by twice the normal amount. Caution is therefore necessary in interpreting small temperature effects.

*Due to internal radiation from the nose fairing.

5. SUPPORT OPERATION

5.1 AFMTC Instrumentation Support

AFMTC instrumentation support during the Able-4 launch is considered good. Coverage obtained was as follows:

a) First-stage telemetry reception on the 228.2 link was received from T + 0 to T + 600 seconds by the Cape and from T + 43 to T + 655 seconds by Grand Bahama Island.

b) Second-stage telemetry reception on the 244.8 link was received from T + 0 to T + 780 seconds by the Cape and from T + 70 to T + 796 seconds by Grand Bahama Island.

c) Additional telemetry coverage was provided by the TLM-18 at TELE-3, which tracked the payload at all intervals, when the payload was visible and the transmitter was on, from launch time to 100,000 nautical miles.

d) Optical coverage was provided by 11 metric, 19 engineering sequential, and 38 documentary cameras. All of the cameras functioned with the exception of one engineering sequential.

e) Radar skin tracking support was provided during launch from the following Cape Canaveral installations: Mod IV tracked from T + 0 to T + 180 seconds, Mod II at Station 1.5 from T + 25 to T + 150 seconds, AN/FPS-16 at Station 1.16 from T + 16 to T + 210 seconds. In addition to the Cape stations, the AN/FPS-16 at Station 3.16 tracked from T + 134 to T + 211 seconds.

5.2 Tracking Operations

The integrated tracking, telemetry, and command radio communication link with the Able-4 vehicle has performed successfully since launch. The payload transmitter was acquired six minutes after launch by the Cape and by Manchester when the payload appeared over the horizon. It was turned off by the Manchester ground station 25 minutes later.

Initial tracking data from the Space Navigation Network proved to be very accurate and reliable. As a result, the machine computation of the vehicle's trajectory made 16 hours after launch has not required further refinement.

Cooperating stations of the worldwide tracking network were Cape Canaveral, Florida; Millstone, Massachusetts; Goldstone, California; Kaena Point, Hawaii; APL, Silver Springs, Maryland; Ft. Monmouth, New Jersey; and the Minitrack station at Blossom Point, Maryland.

All useful data received was angular data. Millstone and Goldstone both obtained good and extremely valuable data. It was necessary to remove the Singapore and Florida stations from ground tracking on 13 March because of their small antennas.

In subsequent weeks the transmitter has been operated on a duty cycle of approximately 10 per cent; for each hour of transmission time, about 10 hours of battery recharging takes place. The only difficulties in the communication link have occurred in the ground stations. Transmitter repair caused the Hawaii station to be idle for a day and a half and high winds at Manchester forced this station to be inoperative briefly. Payload equipment is performing quite well except for the degraded batteries.

5.3 Real Time Trajectory Determination

5.3.1 Preflight Preparation and Data Plan

Prior to launch, a final reference set of closed-loop guided trajectories was computed for a range of lift-off times covering the allowed launch interval. These trajectories included final preflight weight and performance data supplied by TWX from Cape Canaveral, including the changed third stage of the vehicle. The second-stage ground guidance computer was programmed to vary the trajectory systematically throughout the launch interval but not from one launch day to another. Curves of burnout conditions as a function of lift-off time were prepared from these computer runs.

When lift-off time was received during the real-time operation, the nominal burnout conditions were read from the curves for use as a first estimate in the least squares tracking process. These nominal conditions are listed in Table 5-1 and represent the best preflight trajectory for all comparisons with the actual trajectory obtained from tracking data and powered flight reconstruction. Nominal open-loop burnout conditions (independent of lift-off time) were also available in case the second-stage guidance loop was not closed.

Data planned for use in the trajectory determination task at the SpaN Center was as follows:

a) Discrete point, 20 r-dot points and 15 data van points from Cape AGS site.

b) E and A data from Millstone.

c) E and A data from Manchester.

d) E and A data from TELE-3 and NASA Minitrack at Cape.

5.3.2 Trajectory Determination Operations

Initial data available at SpaN after lift-off of the vehicle was from the AGS site. After programming of this data through the IBM 709 computer, it was determined that the data was not valid. Trajectory LS-1 was therefore run with Manchester, Millstone, and TELE-3 data (6 x 6 least squares fit). The first iteration, LS-1, indicated that the flight of the vehicle was near nominal, at approximately 65 minutes after lift-off. Additional data points from Millstone and Manchester were then used in generating trajectory LS-2. Information on initial conditions and sunframe orbital elements was released by SpaN based on LS-2.

For the next 17 hours the process of receiving new observations, revising the trajectory determination, computing new steering data for ground stations, and releasing orbital information was continued. A second set of orbital elements was released at T+9 hours based on LS-3.

Table 5-1. Burnout Conditions.

Quantity	LS-1		LS-2		LS-3		LS-4		Preflight Nominal	(LS-4-Nominal)*
α_o	297.51°	(0.08)	297.51°	(0.07)	297.63°	(0.06)	297.880°	(0.015)	297.52°	+.36°
δ_o	28.26°	(0.05)	28.27°	(0.03)	28.26°	(0.03)	28.251°	(0.02)	28.11°	-.14°
r_o	22,253,567	(23,000)	22,245,208	(18,000)	22,300,638	(12,700)	22,336,111	(7300)	22,275,000 ft	+61,100 ft
V_o	36474.3	(22)	36484.4	(16)	36430.4	(9.5)	36403.6	(5.7)	36,597 fps	-193 fps
β_o	78.08°	(0.15)	77.97°	(0.09)	78.34°	(0.03)	78.281°	(0.004)	75.77°	+2.51°
A_o	92.95°	(0.15)	92.85°	(0.09)	93.17°	(0.03)	93.021°	(0.006)	93.05°	-.03°
V_{eq}	36457.6		36461.2		36450.8		36451.06		36,597	-146 fps

EPOCH: 335.52 sec after lift-off = $13^h\ 05^m\ 42.62^s$ GMT, 11 March 1960

NOTE: Numbers in parentheses are one-sigma values for the uncertainty in the estimated initial conditions.

DEFINITIONS:

α_o = right ascension of burnout point from equinox of date.

δ_o = declination (latitude) of burnout point.

r_o = distance of burnout point from center of earth.

V_o = inertial velocity at burnout.

β_o = angle between geocentric radial to burnout point and inertial velocity vector.

A_o = azimuth of inertial velocity vector from north.

V_{eq} = equivalent velocity (for constant energy) of probe referenced to nominal burnout value of r_o = 22,275,000 ft.

"burnout point" = point on trajectory chosen before flight at arbitrary time of 335.52 sec after lift-off, actually approximately 12.6 sec after burnout.

At T+19 hours and based on the fourth orbit determination, LS-4 was generated. Steering data for the next four days was sent by TWX to ground stations at Manchester, Millstone, Cape, Hawaii, Singapore, Goldstone, and APL. Initial conditions and orbital elements were sent to NASA, Spacetrack, Smithsonian, and JPL. The real-time trajectory task was terminated at T+20 hours.

5.3.3 Results Obtained

Table 5-1 lists the initial conditions for the free-flight trajectory as obtained from LS-1 through LS-4. The time epoch of these conditions is 12.6 seconds after third-stage burnout. The numbers shown in parentheses are one-sigma values for the uncertainty in the estimated initial conditions and were obtained from the covariance matrix in the least square process. Loss of the discrete burnout point from the Cape and of all Cape $\dot{R}$ data left an undesirably large uncertainty in burnout velocity and may make determination of the A.U. more difficult. It had been anticipated that velocity would be known to better than 0.1 ft/sec at the time of LS-4. Subsequent to the real-time task, it was decided that the doppler equipment had locked onto telemetry sidebands and over one-hundred reconstructed Cape doppler points were furnished to the Guidance and Navigation Department. These were used to determine a new trajectory, LS-4B, containing the doppler plus LS-4 data. A fit could be obtained only by introducing an unknown bias determined along with the initial conditions in a 7 x 7 least squares process. The resultant bias was approximately 12 feet per second and is of unknown physical significance. Later data obtained in the following days suggests strongly that trajectory LS-4B is less accurate than LS-4.

Table 5-2 lists the equatorial elements of the escape hyperbola corresponding to LS-1 through LS-4. The elements of the probe orbit about the Sun are given in Table 5-3. It should be noted that the heliocentric elements vary slightly from point-to-point along the orbit due to perturbations of the earth and other bodies. The elements listed in Table 5-3 are quoted at an epoch 70 days from burnout (about one-half way from launch to perihelion)

Table 5-2. Equatorial Elements of Escape Hyperbola.

Quantity	LS-1	LS-2	LS-3	LS-4
a	-10.31 er.	-10.27 er.	-10.40 er.	-10.388 er.
e	1.0989	1.0992	1.0985	1.09870
i	28.40°	28.40°	28.43°	28.399°
Ω	201.29°	201.51°	200.95°	201.518°
ω	72.72°	72.32°	73.62°	73.229°
m	0.00877	0.00889	0.00852	0.00859

Epoch: $13^h\ 05^m\ 42.62^s$ GMT, 11 March 1960.

Definitions:

a = semimajor axis of orbit (earth-radii)
e = eccentricity
i = inclination of orbit plane to equator
Ω = longitude of ascending equatorial node from equinox of date
ω = angle in orbit plane from ascending node to perigee
m = mean anomaly at epoch (radians)

Table 5-3. Heliocentric Orbit* (Ecliptic Elements).

Quantity	LS-1	LS-2	LS-3	LS-4	Preflight Nominal
a	0.8993 A. U.	0.8990 A. U.	0.8999 A. U.	0.89958 A. U.	0.8930 A. U.
e	0.1044	0.1048	0.1035	0.10396	0.1132
i	3.34^{o}	3.34^{o}	3.36^{o}	3.351^{o}	3.37^{o}
Ω	-10.27^{o}	-10.27^{o}	-10.29^{o}	-10.288^{o}	-10.06^{o}
ω	-3.14^{o}	-3.31^{o}	-2.70^{o}	-2.585^{o}	-7.60^{o}
T	151.3 days	151.1 days	151.9 days	151.96 days	145.11 days
Period	311.5 days	311.3 days	311.8 days	311.64 days	308.2 days
Perihelion	0.805 A. U.	0.805 A. U.	0.807 A. U.	0.8061 A. U.	0.792 A. U.
Achelion	0.993 A. U.	0.993 A. U.	0.993 A. U.	0.9931 A. U.	0.994 A. U.

*Osculating elements of heliocentric orbit, quoted at epoch = 70.00 days after T_o = $13^{h}\ 05^{m}\ 43^{s}$, 11 March 1960

Definitions:

Same as for escape hyperbola, except

(1) reference plane is ecliptic and equinox is equinox of 1950.0

(2) T is time from reference date T_o to perihelion

and were obtained by an integration including the perturbing effects of the Earth, Moon, Venus, Mars, and Jupiter. The period about the Sun of LS-2 released 2.5 hours after launch differs from the best subsequent determination by about eight hours.

Detailed information on the last orbit determined is given in Section 5.4.

5.4 Payload Orbit

The definitive observational orbit provides sufficient accuracy for analysis of probe experimental data and for steering of tracking station antennas. Following completion of the tracking of THOR ABLE-4 a definitive metric orbit will be determined, including the results of the A.U. study, and the influence of all observations throughout the flight. The observational orbit has been used as the source of all detailed trajectory printouts and antenna steering data and has remained within 2 fps of observed data throughout the first five weeks of flight.

Information for the definitive observational orbit was developed in two steps:

a) A least squares trajectory program was used to determine a set of injection conditions from approximately 560 observations of angles and range rate obtained by six ground stations during the first 11 hours of flight. This program integrated the differential equations of the probe's orbit by Cowell's method including the perturbations of the Sun, Moon, and Earth oblateness. Radar derivatives were obtained by integration of an auxiliary set of variational equations.

b) The trajectory was then integrated to cover the first 400 days of flight using a similar program including the perturbations of an oblate Earth, the Moon, Sun, Venus, Mars, and Jupiter.

5.4.1 Injection Conditions and Orbital Elements

a) Injection Conditions (rectangular inertial equatorial coordinate system with XY plane the equatorial plane, X-axis positive toward the vernal equinox of date, Z-axis positive toward North Pole of earth spin axis.

X = 9,200,695 ft	$\dot{X}$ = 34,925 fps
Y = -17,391,639 ft	$\dot{Y}$ = 10,102 fps
Z = 10,572,603 ft	$\dot{Z}$ = 1,845 fps

Epoch:

$13^h\ 05^m\ 42.62^s$ GMT (11 March 1960)

b) Equatorial Elements of Escape Hyperbola

a = -10.388 earth-radii	(semimajor axis)
e = 1.09870	(eccentricity)
i = 28.399 degrees	(inclination)
Ω = 201.518 degrees	(longitude of ascending node)
ω = 73.229 degrees	(argument of perigee)
m = 0.00859 radians	(mean anomaly)

Epoch:

$13^h\ 15^m\ 42.62^s$ GMT (11 March 1960)

Reference:

Equator and Equinox of Date

c) Heleocentric Orbit (Ecliptic Elements)

a = 0.89958 A.U.	
e = 0.10396	
i = 3.351 degrees	
Ω = -10.288 degrees	
ω = -2.585 degrees	
τ = 151.96 days	(time from T_o to perihelion)

Definition:

Period = 311.64 days

Perihelion = 0.8061 A.U.

Aphelion = 0.9931 A.U.

Oscillating elements of orbit quoted at Epoch = 70.00 days after T_o

T_o = 13^h 05^m 42.63^s GMT (11 March 1960)

Reference Equinox of 1950.0

For the majority of the angular observations (Millstone and Goldstone) residuals of 0.5 to 2.0 mils were obtained. The rms range rate residual was 1.10 fps for Manchester and 1.130 fps for Hawaii. The standard errors of the heliocentric elements of the THOR ABLE-4 orbit were computed from the covariance matrix of the least square trajectory determination with the following results:

σ_a	= 8.0×10^{-6} A.U.	(semimajor axis)
σ_e	= 10.0×10^{-6}	(Eccentricity)
σ_i	= 0.00027^o	(inclination)
σ_Ω	= 0.00004^o	(Longitude of mode)
σ_ω	= 0.0013^o	(Argument of Perihelion)
σ_p	= 6.1 minutes	(Period)

Neglecting any uncertainty in the size of the astronomical unit, these sigmas are equivalent to:

$\sigma_{Perihelion}$ = 1320 nautical miles

$\sigma_{Aphelion}$ = 15 miles

The above standard errors should be degraded slightly due to small undetected biases and correlations in the data, neglected in computations of the sigmas.

5.4.2 Details of THOR ABLE-4 Orbit

Figure 5-1 shows an earth-centered projection (top view) of the THOR ABLE-4 escape trajectory on the equatorial plane. The projection of the Moon's orbit, the Earth's velocity vector about the Sun, and the direction of sunlight are also shown.

In Figure 5-2 the trajectory is projected on the surface of the Earth for the first two days of flight. The projection for subsequent days will be a straight line approximately parallel to the equator. The latitude of the probe will vary from day to day as shown in the plot of right ascension versus declination (geocentric latitude) of Figure 5-3.

The asymptotic velocity of the probe on its escape hyperbola is 8047 fps. The excess velocity of the probe over escape velocity was 900 fps at a geocentric distance of 22,275,000 feet. On escaping from the Earth the vehicle began to move on the heliocentric orbit illustrated in Figure 5-4. The orbit projected on the ecliptic plane along with the orbit of the Earth and the projection of Venus' orbit. The projection of the spin axis of the vehicle on the ecliptic plane is also indicated.

The distance of the probe from the Earth as a function of time is given in Figure 5-5 for the first 200 days of the flight (note that the distances are in nautical miles rather than statute miles).

Figure 5-6 gives the velocity of THOR ABLE-4 relative to the Earth as a function of time. The distance of the vehicle from the Sun versus time is shown in Figure 5-7.

The radar curves for all stations will be similar from day to day and will change in shape slowly. The range rate seen by a station will be that for center of the Earth (Figure 5-6) with a daily oscillation in amplitude as large as 1500 feet per second due to the rotation of the Earth superimposed on the slow trend. There will be a much smaller additional term due to the monthly motion of the Earth about the Earth-Moon barycenter.

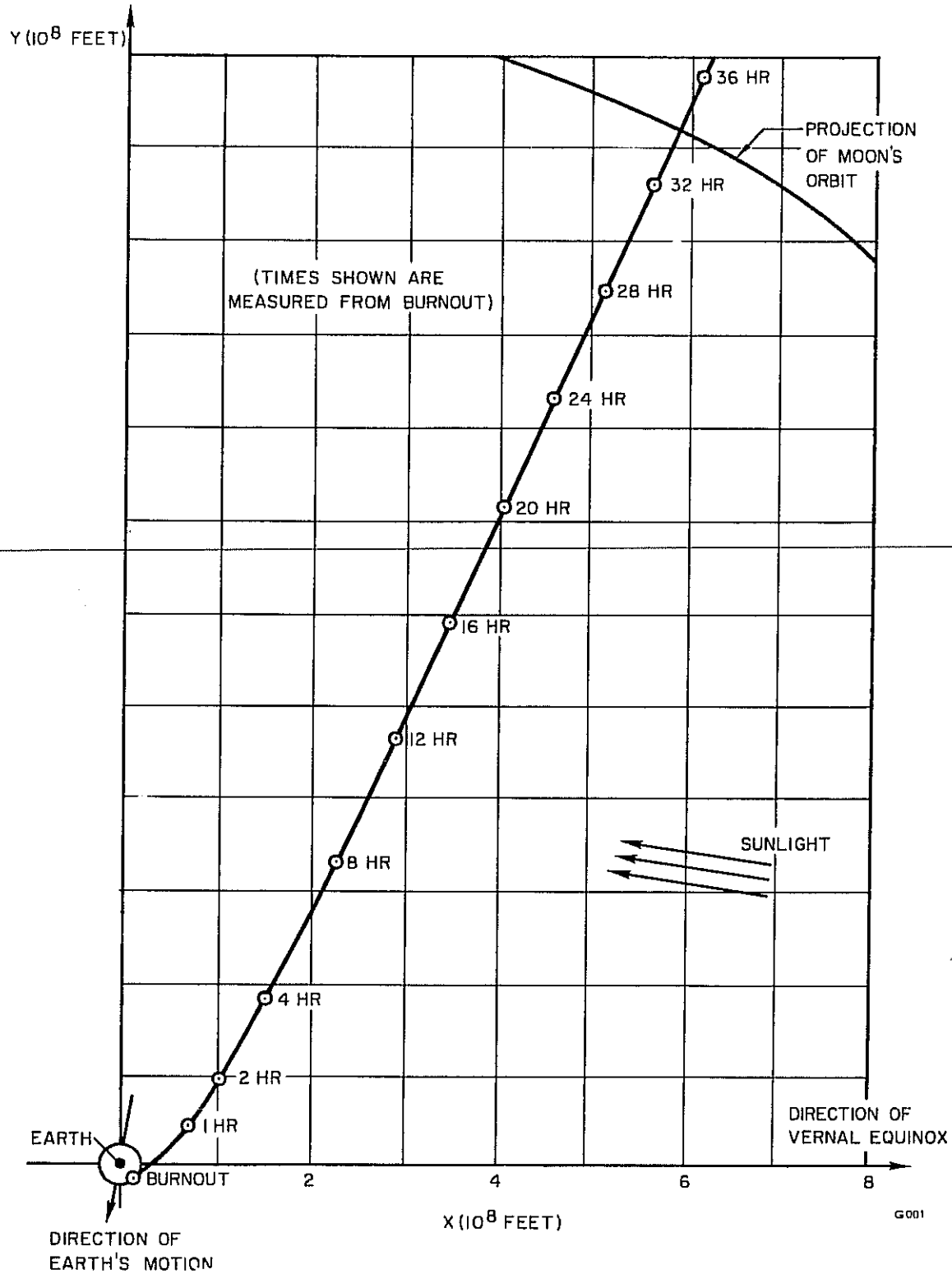

Figure 5-1. Projection of Thor Able-4 Trajectory on Equatorial Plane (first 36 hour of flight).

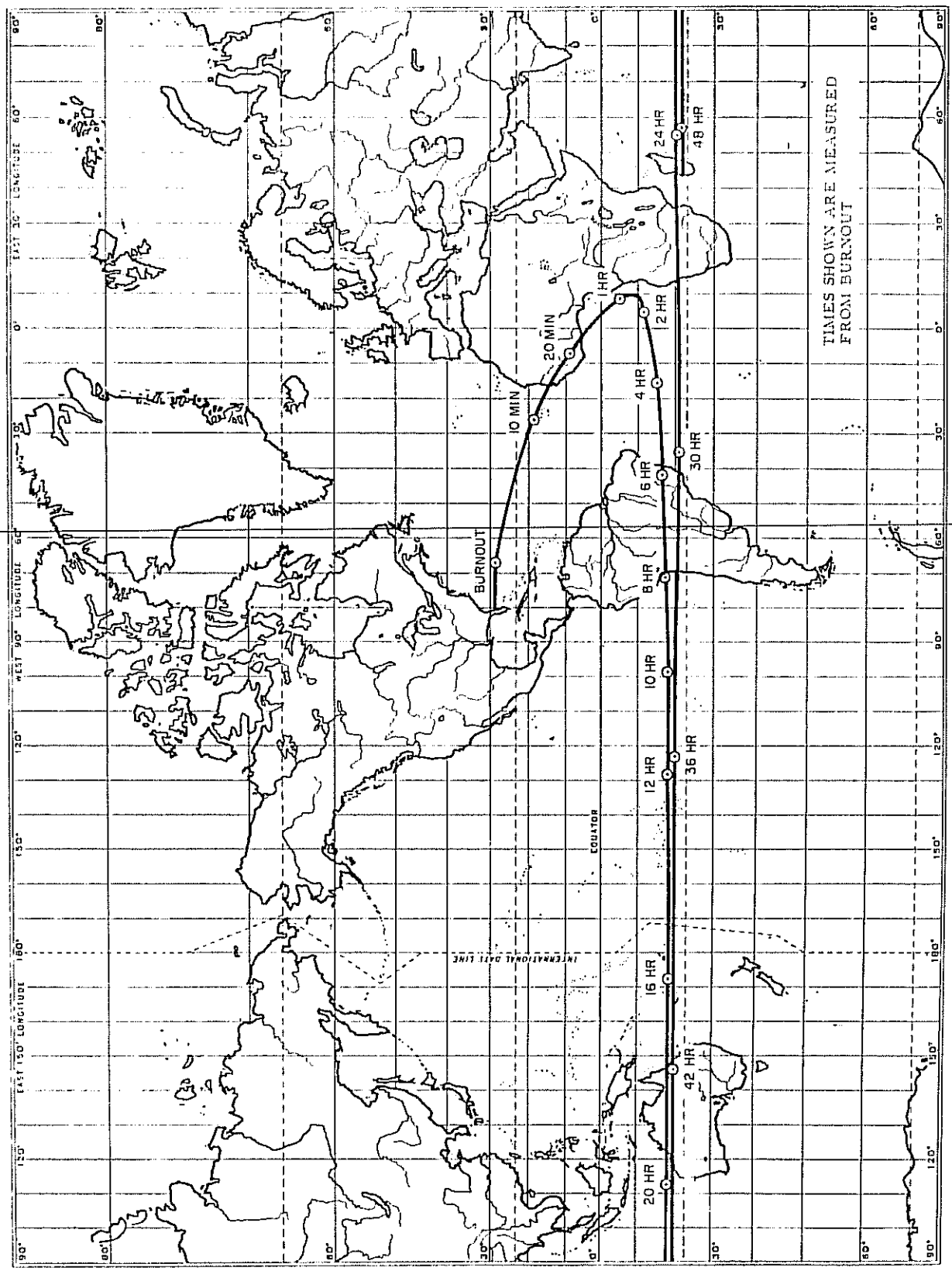

Figure 5-2. Thor Able-4 Trajectory Projected on the Earth for First Two Days of Flight.

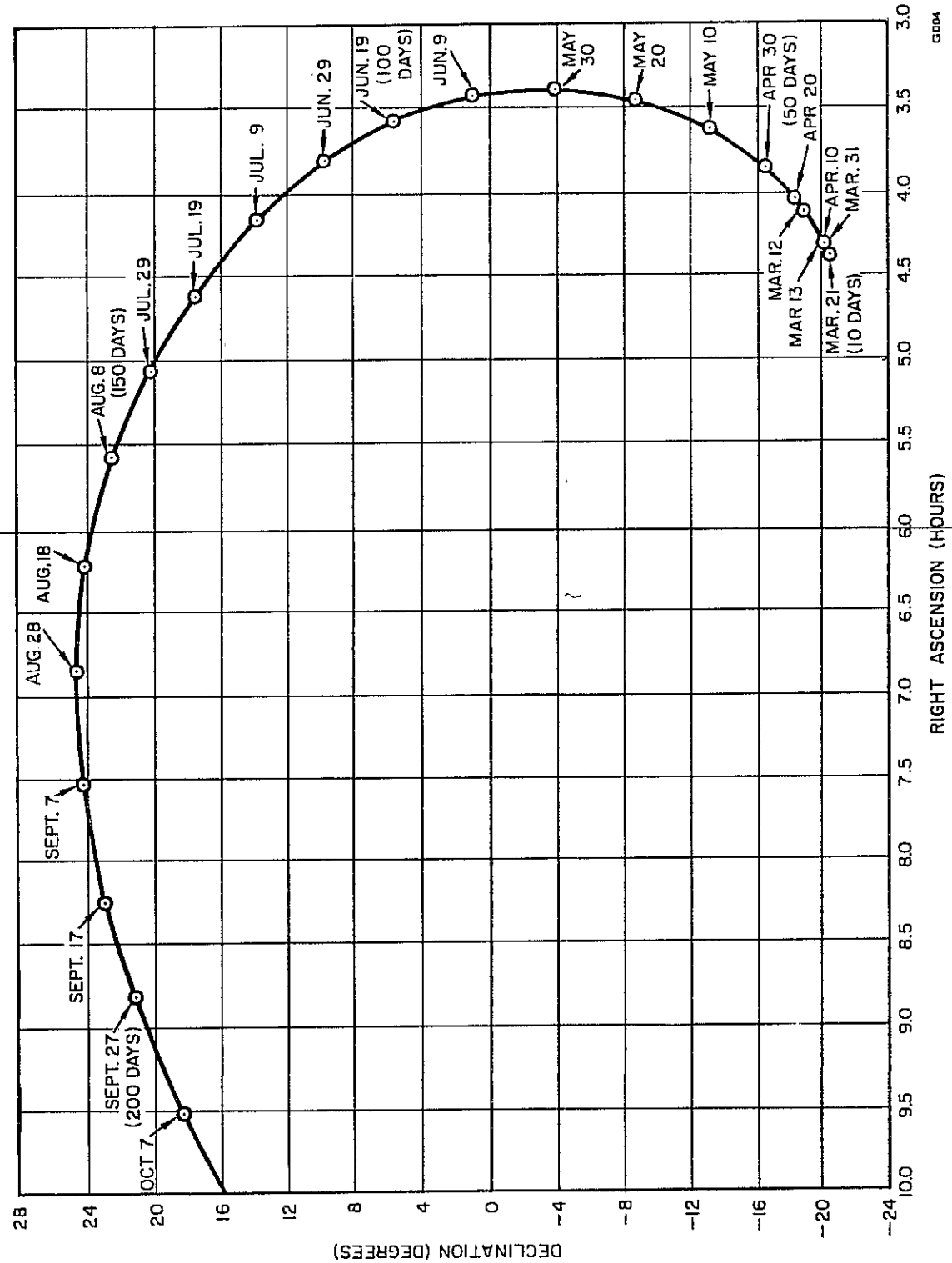

Figure 5-3. Right Ascension Versus Declination for Thor Able-4.

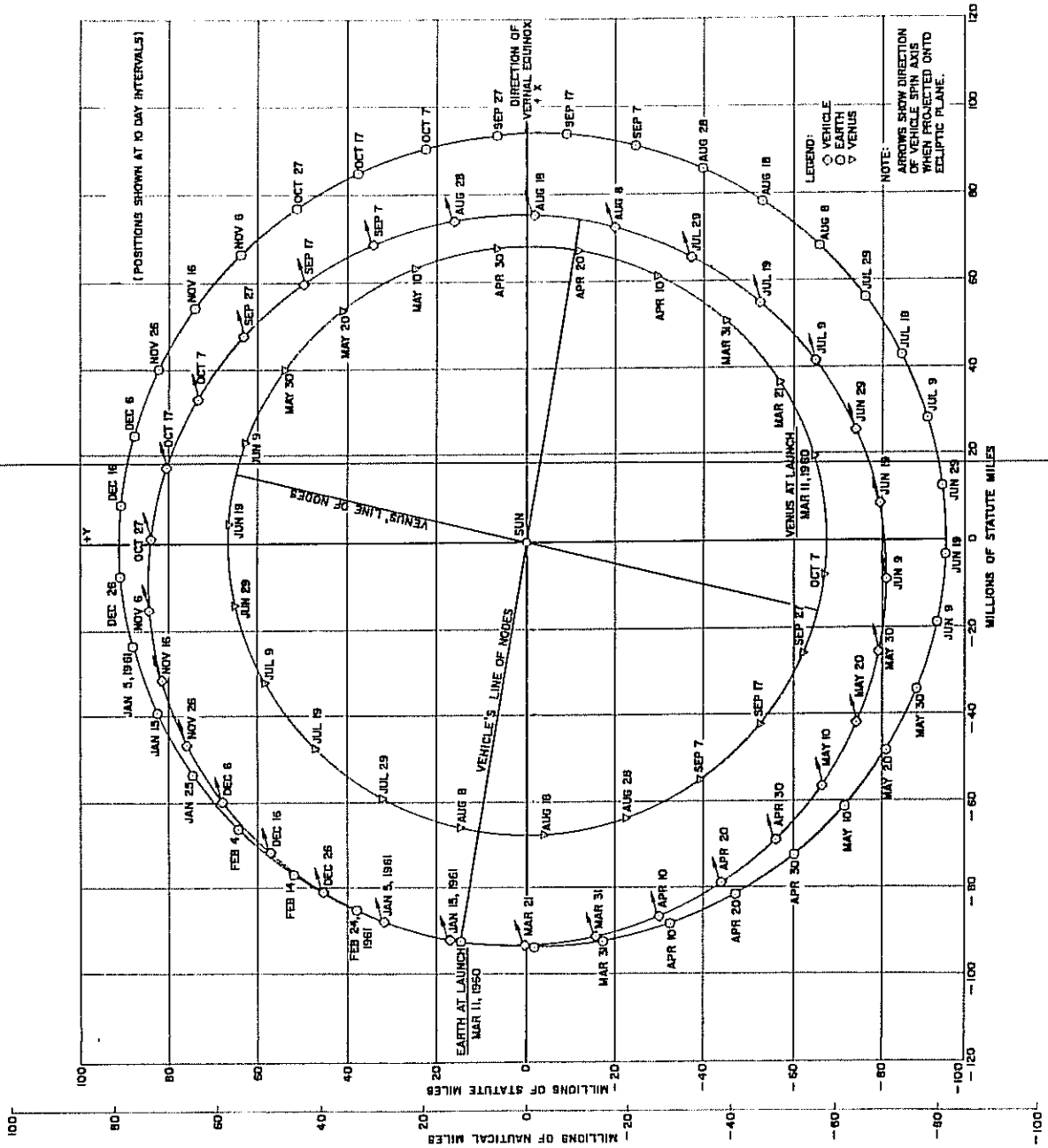

Figure 5-4. Ecliptic Plane View of Thor Able-4 Orbit.

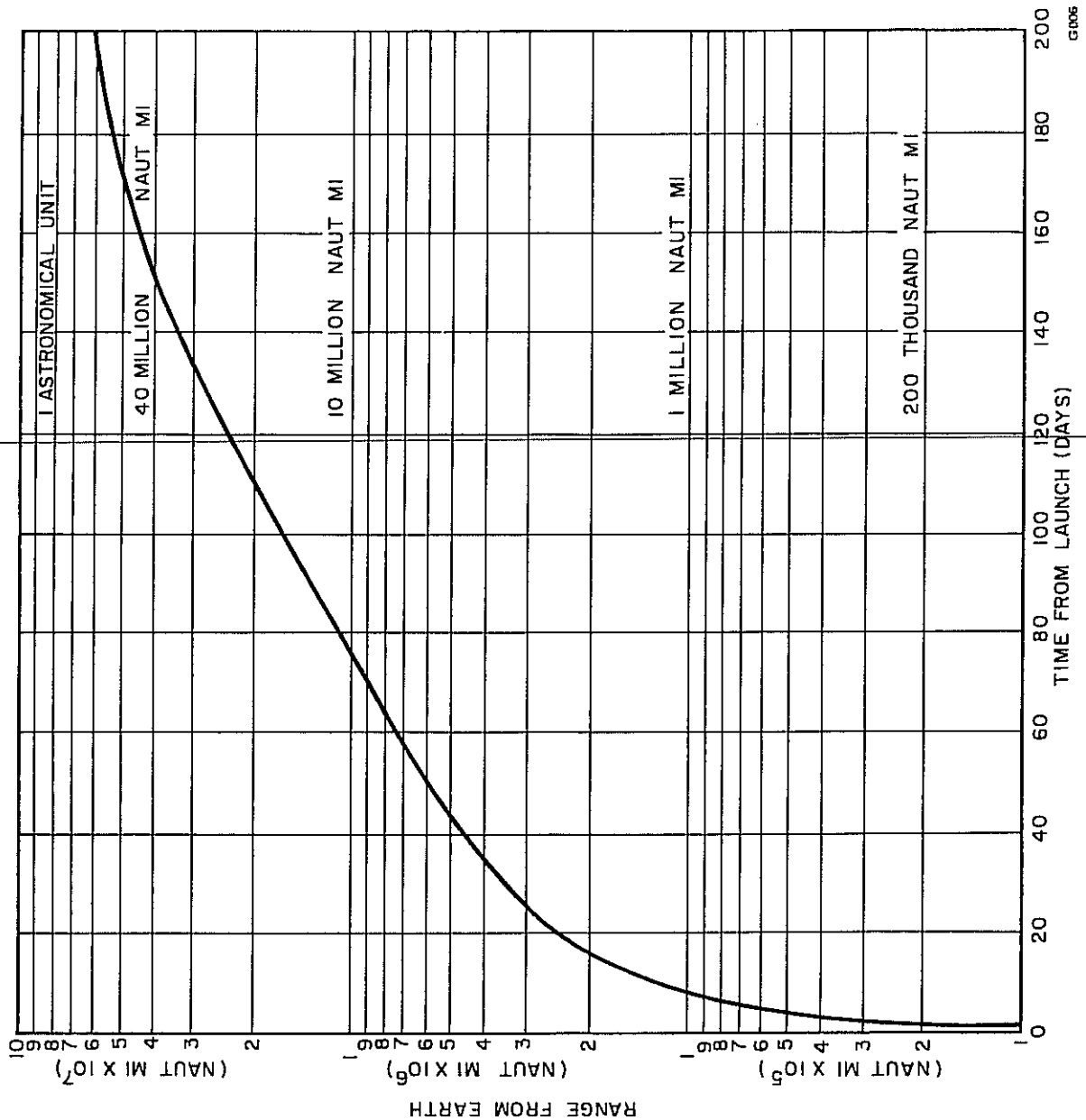

Figure 5-5. Range from Earth to Venus Versus Time from Launch.

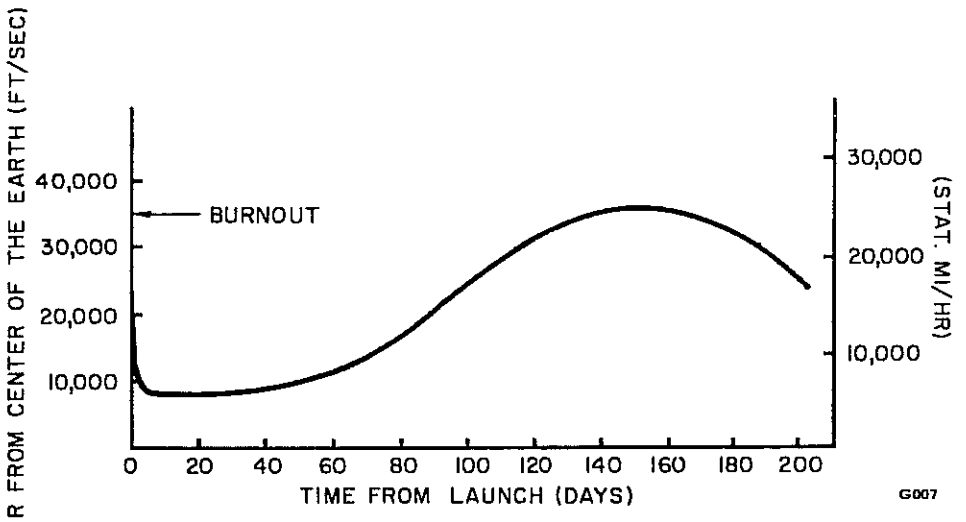

Figure 5-6. Range Rate from Center of Earth Versus Time from Launch.

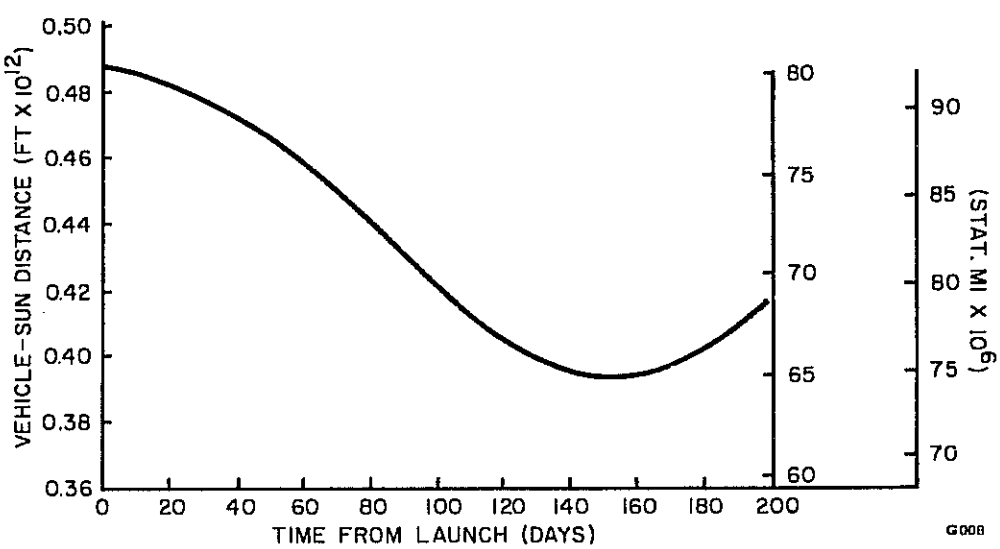

Figure 5-7. Vehicle-Sun Distance Versus Time from Launch.

As the Earth moves around the Sun the times of rise and set of THOR ABLE-4 at Hawaii and Manchester will vary as illustrated in Figure 5-8. Since the probe's orbit is inclined to the ecliptic, the Sun-Earth-probe angle does not become less than 29 degrees during the first 200 days of the flight. The variation of this angle with time is shown in Figure 5-9.

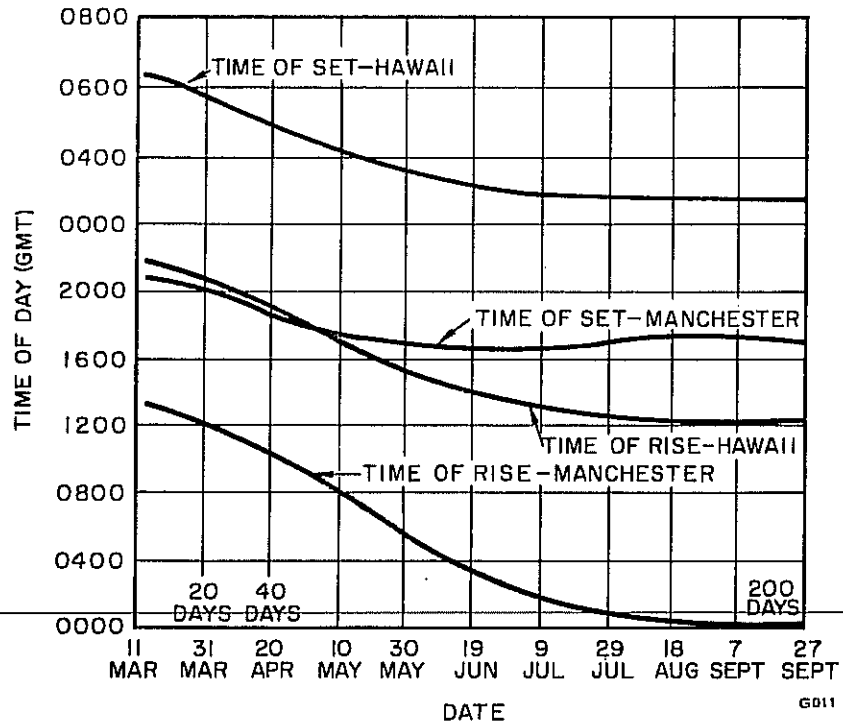

Figure 5-8. Rise and Set Times for Manchester and Hawaii.

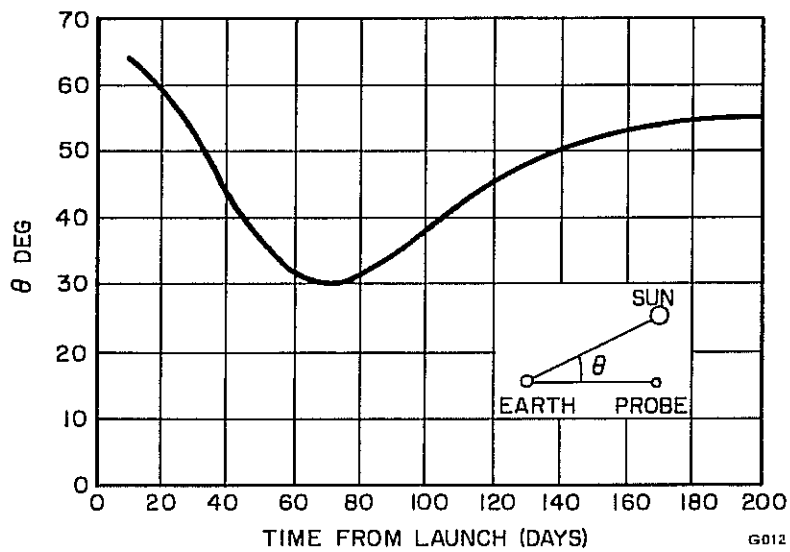

6. PRELIMINARY SCIENTIFIC RESULTS

6.1 Astronomical Unit

The astronomical unit (AU) is the fundamental unit of length for the location of objects in space. One AU is equal to the length of the semimajor axis for the earth's orbit about the sun. Results of existing methods for measuring the AU are inconsistent; measurement by a different means will prove quite valuable. The method for AU measurement used by the ABLE-4 experiment requires that the position and velocity of the space vehicle be accurately determined at two widely separated times in its trajectory.

The initial conditions for the free-flight trajectory as obtained through LS-4 give a value for aphelion = 0.9931 AU and perihelion = 0.8061 AU. It had been anticipated that velocity would be known to better than 0.1 ft/sec at the time of LS-4. Loss of the discrete burnout point from all r-dot data left an undesirably large uncertainty in burnout velocity and may make the determination of the AU more difficult.

The figures given for perihelion and aphelion have been converted from AU to nautical miles assuming perfect knowledge of the number of nautical miles in one AU. Although the orbit is known quite well in AU, measurement of the AU must await data several months from launch when the derivative of radar r-dot with respect to size of AU becomes significant.

6.2 Micrometeorite Measurements

The micrometeorite experiment is designed to measure the distribution of cosmic dust in the ecliptic between the orbits of Venus and the earth. Impacts of micrometeorites on an acoustically isolated surface of 0.04 square meter area were detected by means of a piezoelectric transducer. The pulsed signal from the transducer was amplified, shaped, and two separate pulse amplitudes were stored in the "telebit" unit. The lower threshold pulse level is sensitive to impacts of dust particles with masses greater than 1.2×10^{-10} grams as estimated from a momentum

calibration and an average impact velocity of 30 km/sec. The upper threshold level was 1.7×10^{-9} grams. From the lower and upper threshold level data the mass distribution of cosmic dust could be computed. Preliminary data from the experiment has been received for the interval from 11 March through 24 April 1960, shown in Table 6-1. Apparently the experiment is not operating satisfactorily as evidenced from the data which indicates that actually three or less impacts were recorded during the first three and a half days after launch, and that there were two cases of erratic operation resulting in counter saturation. The experiment appears to have functioned between 27 March and 2 April. The available data and a preliminary analysis is given below.

Table 6-1. Micrometeorite Counter Readings.

Date	Zebra Time		Counter	
1960	Hour	Minutes	A	B
11 March	13	25	045	7
14 March	22	40:35	045	7
14 March	22	41:11	127	7
20 March	18	15	127	7
20 March	22	32	000	7
27 March	17	15	000	7
29 March	13	40	001	7
29 March	17	01	003	7
2 April	12	41	006	6
3 April	12	47	007	6
14 April	22	49	007	7
18 April	15	30	127	7
24 April	--	--	127	7

The two counters in the "telebit" unit recorded data using a binary system. Counter A which recorded both lower and upper levels used a scale of 4 and could count to 127 before recycling after a total of 512 pulses. Counter B was on a scale of 2 and recycled after 16 upper level pulses. Both

storage units showed multiple counts during the launch phase including payload and third-stage separation. This was expected. After injection the A counter reading was 45, and the B counter reading was 7. From the time of injection until 2240 on 14 March no change in count was recorded.

At 2241:11 on 14 March in an interval of 36 seconds the A counter was filled to capacity. This may have resulted from the shift accumulator getting stuck in the "one" digit position and loading up all the binaries during operation of the shift register.

On 2 April the B counter reading went to 6 with a corresponding change in the lower pulse level count. A series of 13 to 15 consecutive upper level counts or an effect from operation of the under-voltage control may have caused this change.

Thus, there is evidence of faulty operation of the equipment associated with the micrometeorite experiment. It is doubtful that any useful data will be forthcoming from the experiment.

6.3 Ion Chamber and Geiger Counter

The geiger counter and ionization chamber experiments uncovered significant data during the period of solar activity which began 31 March. The response of the instruments to five or possibly six cases of flares occurring during this period can be identified with low energy solar cosmic rays. The largest cosmic ray burst occurred on 1 April, and was associated with a Class 3+ flare beginning at 0830 Greenwich mean time. Another major cosmic ray burst occurred on 5 April and was associated with a major radio disturbance. Up to this time, this burst has not been identified with a particular flare.

Some of the unusual phenomena associated with the activity of 1 April, as observed by the Minnesota experiment or on the earth are:

a) During these groups of phenomena the counting rates range from values just detectably above galactic background to fluxes 10 times background.

b) The differential energy spectrum as measured within a 0.5 to 5 grams per square centimeter of load shielding has a form CE^{-4}.

c) Decrease in particles in space after a solar event follows a law $i_o t^{-1.9}$. The decay seems more rapid than the 1.5 power predicted by simple diffusion.

d) Three cosmic ray events produced polar ionospheric changes.

e) Although all events have been analyzed on the basis of a proton flux only, the presence of a smaller flux of α particles cannot be excluded.

f) A large Forbush decrease occurred 31 March to 1 April. The decrease at sea level at high latitude was ten percent, and in balloons the ionization decrease was twenty-five percent.

g) On 31 March and again on 4 April, the high ion/count ratio gave evidence for soft Bremsstrahlung from electrons striking THOR ABLE-4. The intensity in the ion chamber corresponds to the electron flux of slightly less than 1,000,000 per square centimeter per second at 50,000 electron volts.

h) During the period of 2 through 7 April following an initial "dumping" on 1 April, the outer Van Allen radiation belt in the earth increased in intensity from ten to forty times normal at ranges 1000 km above the surface, as observed by the Explorer VII earth satellite.

It can be said conclusively that the increase [(h) above] in 50,000 electron volt electrons observed 2 through 7 April was not due to direct solar ejection since the flux observed by the payload in space was only 10^{-4} of that appearing 1000 kilometers above the earth's surface. It seems likely that the weak electron flux observed on the ATLAS ABLE-4 on 31 March and 4 April represents the high energy end of a solar plasma cloud spectrum associated with the magnetic storm and with the Forbush event.

6.4 Magnetometer

The magnetometer data observed by THOR ABLE-4 during the first 20,000 miles fitted the theoretically predicted dipole magnetic field of the earth. At a distance greater than 24,000 miles from the center of the earth, the analysis of the magnetometer data shows an increasing deviation from the predicted dipole magnetic field. The largest deviation is observed at about 40,000 miles. The deviation can be explained if a current is postulated which circles the earth at a distance of 40,000 miles. If this current has a cross section of about 12,000 miles and is comprised of a total flux of 5,000,000 amperes, the deviation from the dipole field is adjusted and fits the magnetometer data very reasonably. The ring current appears to be dissociated from the Van Allen radiation belts. Thus, the ring current appears to be a third major dynamical element of charged particles surrounding the earth, in addition to the inner and outer Van Allen radiation belts.

The second observation of importance made by the magnetometer was existence of an intense zone of disturbed magnetic field occurring at some 40,000 to 60,000 miles altitude. This region has been postulated to be the boundary between the earth's magnetic field and magnetic fields which accompany plasma emitted from the sun. Data appears to indicate that this region is twice as far from the earth as had been previously supposed.

The third set of observations made by the magnetometer is the measurement of the interplanetary magnetic field. Correlation with the cosmic ray experiments are in progress, particularly concerning the unusual solar activity which began on 31 March.

6.5 Cosmic Ray Telescope

The preliminary result obtained from the cosmic ray telescope during the time period within which the payload traveled to a distance of approximately 8,000,000 km from the earth is worthy of discussion. Beginning 31 March, solar activity rapidly increased with many solar flares, radio

noise bursts, etc., over the period of ten days. On 31 March, a Forbush decrease occurred at the earth and at the payload. The decrease at 5,000,000 km from the earth was at least as great as the decrease observed at the earth itself. This observation appears to invalidate existing theories which attempt to explain Forbush decreases, and are founded on a postulate requiring proximity of the earth and of its magnetic field.

The direct detection of particles accelerated in solar flares was observed. Not only were protons and electrons detected on 1 April, but gamma rays as well were counted during this outstanding event. This shows that solar flare particles producing the ionization in the earth's polar atmosphere cannot be stored in the geomagnetic field or at the sun.

Evidence has been obtained supporting the assumption of solar production of energetic electrons by process other than solar flares. Bremsstrahlung were measured for many days during which the sun was relatively quiet. The objectives of the experiment include detection of all particles accelerated to high energies at the time of unusual solar events. Thus a temporary 24-hour watch has been established to receive data from stations all over the world observing solar and solar related phenomena. In case an unusual event such as a solar flare is detected, communication channels are available whereby earth stations recording telemetering sequences from the payload will be alerted to obtain additional data at these times. On two occasions changes were made in the tracking schedules to explore the occurrences of unusual solar activities. Such special transmissions have proved to be extremely valuable scientifically.

6.6 Aspect Indicator

The aspect indicator was designed to measure the phase relationship between the output of a photoelectric diode "sun scanner" and the spin coil magnetometer. The primary purpose of this information was to assist in the determination of electric currents in space, the magnetic field of planets, and the characteristics of radio propagation. However, from the time of lift-off, the indications received provided no usable information.

APPENDIX

CONFIGURATION OF THOR ABLE-4 VEHICLE

The THOR ABLE-4 test vehicle consists of three stages and a payload. The three stages impart sufficient velocity to the payload to enable it to escape the earth's gravitational field and enter into an elliptical orbit around the sun. The configuration of the stages follows.

A. Stage I

The first stage utilizes a standard Thor missile with the inertial guidance system removed and the control system modified to accommodate the dynamics of the three-stage missile. Guidance is accomplished by means of roll and pitch programmers. The Rocketdyne liquid propellant engine cutoff occurs upon incipient exhaustion of either propellant, i.e., upon actuation of a fuel pump inlet pressure switch. In order to increase performance, RJ-1 fuel is used.

B. Stage II

The second stage is divided into two main sections: propulsion and guidance. The propulsion section contains two propellant tanks, a helium tank and pressure system, two roll control nozzles, and the rocket engine. The guidance section contains a guidance transponder, the flight control system, power supply, and an FM/FM telemetry system.

Propulsion for the second stage is provided by an Aerojet-General model AJ10-101A liquid engine. Pitch and yaw control is achieved by gimbaling the second-stage engine thrust chamber. Roll control is achieved by the "on-off" discharge of high pressure helium through the roll control nozzles. Spin control is provided by six Atlantic Research Corporation rockets. The spin rockets are ignited two seconds after second-engine cutoff and impart a 2.5 revolutions per second spin to the second stage, third stage and payload. The second-stage guidance system operates on a closed-loop basis in conjunction with the STL Advanced Guidance Studies

ground station at Cape Canaveral. Range rate is obtained by two-way doppler measurement. Range is obtained by measuring the round-trip delay in subcarrier modulation. The airborne guidance equipment is used for both steering and engine shutdown. Attitude changes of the test vehicle will be effected by on-off steering using constant rate turns. Only discrete commands will be sent to the second stage from the AGS station. The command link incorporated in the airborne equipment contains six tone channels and has the capability of receiving 15 different commands.

The test vehicle will respond to commands in any given sequence. Except for the shutdown command, transmission of all commands are locked out on the ground two seconds prior to predicted shutdown time. At Stage II shutdown, the airborne guidance transmitter electrical power is cut off.

C. Stage III

The third stage was the same as that used on Able-1 and Able-3, an Allegheny Ballistics Laboratory X248-A4 solid-propellant rocket engine. Trajectory deviation due to thrust misalignment are minimized by the spin stabilization imparted to the vehicle during Stage II spin-up. Both Stages III and IV are covered by an aerodynamic nose fairing jettisoned shortly after Stage I/II separation.

D. Payload

The payload structure is a 26-inch spheroid, flanked by four solar paddles equally spaced around the equator. The spheroid is composed of a central platform, a support structure, a lower cover and an upper cover. The support structure consists of four radial extruded beams terminating at the paddle hinges. The central platform is constructed of Fiberglas honeycomb and acts as the mounting platform for the electronic equipment and the storage batteries.

The solar cell paddles consist of a light aluminum spar with modular pallets of solar cells attached. The paddles are canted in order to

maximize the average number of cells exposed to the sun's radiation. The paddles also act to increase the roll moment of inertia in lieu of a larger diameter sphere.

The electronic components are powered by storage batteries charged by the effect of the sun's radiation on the solar cells.

The electronic equipment mounted in the payload consists of the following:

a) Sensors for measurement of space environment

b) Telemetry transmitter (and Doppler system transponder)

c) Doppler receiver and Command system

d) Digital telemetry unit

e) Power converter

The Doppler/Command system in the payload is used for active tracking during third-stage operation and free flight, and for transmission of commands to the payload. Desired commands are generated at the ground station by phase modulation of a subcarrier with various pulse sequences. The ground tracking stations have the capability to command the transmitters in the payload to turn "on" or "off", control the telemetry rate and change receiver parameters.

The method of temperature control employed is to coat the payload in a nonuniform manner, taking into account the known sun look angle of the payload during the flight. Such a coating results in the absorptivity-to-emissivity ratio of the spinning vehicle being precisely the value needed to bring the mean payload temperature to the required temperature. Differing sun look angle histories for different launch days result in slight modifications to the coating pattern. The modifications are accomplished by application of decal coatings of various materials. The solar cells will be cooled by raising the long wavelength emissivity of the area by means of thin glass plates. The experiments carried by the payload will

be used to obtain data on the space environment encountered. The experiments are as follows:

a) Astronomical Unit

b) Micrometeorite Flux

c) Ion Chamber and Geiger-Muller Tube

d) Magnetic Field Measurement

e) Cosmic Ray

f) Aspect Indicator

g) Temperature Measurements

h) Voltage Measurements

More detailed information concerning the test vehicle and the experiments may be found in the Detailed Test Objectives for THOR ABLE-4 (TR-59-R002-00595, revised January 1960).

DISTRIBUTION

STL

B. N. Abramson
R. M. Acker
S. Altshuler
A. R. Anchordoguy
P. N. Anderson
R. C. Anderson
H. O. Asbury
G. E. Bagley
M. V. Barton
R. R. Bennett
J. G. Berry
E. K. Blum
R. C. Booton
M. E. Brady
H. S. Braham
B. M. Britain
R. Bromberg
B. A. Bunch (8)
W. C. Carlson
J. Cavoto
W. J. Chalmers
G. S. Cherniak
S. R. Coombs
R. C. Danta
R. B. Davis
R. D. DeLauer
P. Dergarabedian
E. B. Doll
A. F. Donovan
W. M. Duke
J. R. Dunn
L. G. Dunn
M. Fiegen
O. O. Fiet
W. A. Finley
S. W. Fordyce
H. D. Freeman
P. F. Gilmore
P. F. Glaser
G. J. Gleghorn
R. D. Gloor
M. Goldman
M. D. Gorman
A. F. Grant, Jr.
C. Graves
F. K. Guest
W. M. Harrison
H. T. Hayes
C. Heald
W. B. Hebenstreit
W. Heller
J. R. Hickey
L. A. Hoffman
J. E. Holland
R. H. Hornidge
R. E. Hughes
J. Jurmain
A. Kaplan
J. M. Kelso
J. B. Kendrick
J. S. S. Kerr
P. Klein
C. E. Lane
L. K. Lee
R. Lipkis
H. Low
R. F. Mettler
A. B. Mickelwait
F. S. Mosher
R. B. Muchmore
G. E. Mueller
W. Northwood
A. Oswald
R. A. Park
K. E. Patt
C. Pittman
N. S. Pixley
C. S. Powers
G. Reiter
A. Rosenbloom
W. T. Russell
H. A. Samulon
J. Sanders

DISTRIBUTION (Continued)

W. H. Schilling
J. R. Sellars
J. M. Seehof
W. F. Sheehan
Y. Shibuya
F. A. Smith
G. E. Solomon
C. P. Sonett
E. R. Spangler
I. Spielberg
I. J. Spiro
R. G. Stephenson
J. E. Taber
J. W. Thatcher (6)
A. K. Thiel
E. H. Tompkins
E. R. Toporeck
N. W. Trembath
W. Tydon
J. E. Vehrencamp
R. L. Walquist
W. C. Whiteside
R. K. Whitford
V. R. Widerquist
R. R. Wilde
B. A. Wilder
H. Y. Wong
L. Wong

STL Library (2)

Air Force

WDZJP Maj J. S. Smith, Jr. (3 + 3 Hq AF + 10 NASA)
WDGMI Lt Col T. Morgan (5)
WDSOT* Library (50 + 2 reproducible)
WDZT Lt Col R. L. Dennen
WDTR Col L. F. Ayres

Agencies*

Aerojet General Corporation (2)
Douglas Aircraft Company (8)
Rocketdyne (2)
University of Chicago (3)
University of Minnesota (3)

* Via transmittal letter